Anthropogenic perturbations to the fate of terrestrial organic matter in a river-dominated marginal sea

Article *in* Geochimica et Cosmochimica Acta · July 2022

DOI: 10.1016/j.gca.2022.07.012

Chenglong Wang
Nanjing University

Chuchu Zhang
Nanjing University

Guodong Jia
Tongji University

Qian Yu
Nanjing University

Available online at www.sciencedirect.com

ScienceDirect

Geochimica et Cosmochimica Acta 333 (2022) 242–262

Geochimica et Cosmochimica Acta

www.elsevier.com/locate/gca

Anthropogenic perturbations to the fate of terrestrial organic matter in a river-dominated marginal sea

Chenglong Wang [a,b], Chuchu Zhang [a,c], Yameng Wang [a,c], Guodong Jia [b], Yaping Wang [a,d], Chun Zhu [e], Qian Yu [a], Xinqing Zou [a,c,*]

[a] School of Geographic and Oceanographic Sciences, Ministry of Education Key Laboratory for Coast and Island Development, Nanjing University, Nanjing, China

[b] State Key Laboratory of Marine Geology, Tongji University, Shanghai, China

[c] Collaborative Innovation Center of South China Sea Studies, Nanjing University, Nanjing, China

[d] State Key Laboratory for Estuarine and Coastal Research, School of Marine Sciences, East China Normal University, Shanghai, China

[e] ExxonMobil Upstream Integrated Solutions Company, 22777 Springwoods Village Parkway, Spring, TX, USA

Received 5 November 2021; accepted in revised form 11 July 2022; Available online 16 July 2022

Abstract

River-dominated ocean margins (RiOMar) are major terrestrial organic carbon (OC_{terr}) repositories that play an important role in the global carbon cycle. However, riverine inputs of sediment and associated OC_{terr} have decreased substantially due to intensifying human activity. Thus, studying OC_{terr} processing during transport to and within RiOMar is crucial. The East China Sea (ECS) receives reduced sediment loads from the Changjiang River (CJR), which is compounded further by the impoundment of the Three Gorges Reservoir. Here, we examined the CJR-ECS source-to-sink system to understand the fate of OC_{terr} in a typical RiOMar. We analyzed the sedimentary properties (grain size and the specific surface area), bulk organic carbon properties (C/N ratio and $\delta^{13}C$), and molecular biomarkers (*n*-alkanes and GDGTs) of riverine suspended particulate matter (SPM) and surficial marine sediment collected in 2006 and 2018. The C/N ratio, $\delta^{13}C$ value, and short-chain *n*-alkanes abundances in the riverine SPM indicate that phytoplankton productivity could be an important source of OC_{terr} in the basin due to the reduced sediment loads. Seabed erosion occurred in the estuarine–inner shelf areas of the ECS as a result of reduced riverine inputs, which resulted in a change in the distribution of sedimentary OC_{terr}. The reduced total organic carbon content and *n*-alkanes abundance are indicative of the low sedimentary OC_{terr} content. Variations in GDGT-based indices are further manifestation of reduced sediment load, as they show increased in situ production of GDGTs. Spearman correlations indicate that the biomarker abundances were positively correlated with silt, which is in accordance with silt being easily shaped by hydrodynamic sorting. Biomarker abundances along four estuarine–inner shelf transects also exhibited pronounced along-shore or cross-shelf OC_{terr} transport. Furthermore, the relationship between the biomarkers and sedimentary properties indicates that mineral protection plays an important role in regulating the fate of OC_{terr} on continental margins. Therefore, variations in riverine inputs and the sedimentary environment caused by anthropogenic perturbations have affected the abundance, distribution, composition, and transport of sedimentary OC_{terr} in the study area. These findings can be applicable to other RiOMar, as humans continue to shape riverine inputs globally.

Keywords: Terrestrial organic carbon; Molecular biomarkers; Anthropogenic perturbations; Riverine input; Hydrodynamic sorting; River-dominated ocean margins

* Corresponding author at: School of Geographic and Oceanographic Sciences, Ministry of Education Key Laboratory for Coast and Island Development, Nanjing University, Nanjing, China.

E-mail address: zouxq@nju.edu.cn (X. Zou).

https://doi.org/10.1016/j.gca.2022.07.012

1. INTRODUCTION

Organic carbon (OC) burial in marine sediment has been the main long-term sink for atmospheric CO_2 across geological timescales, due to its role in storing CO_2 in the geosphere (Berner, 1990; Hedges et al., 1997; Blair et al., 2004). Ocean margins are hotspots for OC burial (Bianchi et al., 2018), accounting for up to 80% of OC burial in modern oceans (Burdige, 2005). In particular, river-dominated ocean margins (RiOMar), such as river deltas, play a critical role in OC burial (Burdige, 2005). This is due to their high terrestrial OC (OC_{terr}) inputs, biological productivity, and sedimentation rates (McKee et al., 2004; Bianchi and Allison, 2009). >200 Tg C yr^{-1} of OC_{terr} is transported to RiOMar via rivers, but approximately 55–80% of this OC is remineralized (Blair and Aller, 2012). The fate of OC_{terr} in the ocean has intrigued scientists for decades, earning the apt classification of 'geochemical conundrum' (Hedges et al., 1997). Understanding the delivery, dispersal, and cycling of OC_{terr} in the RiOMar is important and highly relevant in the context of the global marine carbon cycle (Berner, 2004; Bianchi, 2011; Blair and Aller, 2012; Wei et al., 2020).

Despite substantial progress over recent decades and numerous explanatory hypotheses, mechanisms underlying this 'geochemical conundrum' have not been fully illuminated. It is traditionally hypothesized that intrinsic chemical composition (Sinninghe Damsté et al., 2002a), oxygen exposure time (Hartnett et al., 1998; Keil et al., 2004), mineral protection (Mayer, 1994; Blattmann et al., 2019; Hemingway et al., 2019), and organo-metal complex formation (Lalonde et al., 2012; Shields et al., 2016; Zhao et al., 2018) are the main factors influencing OC_{terr} in the RiOMar. However, uncertainties persist regarding the fate of OC upon burial. These uncertainties can be attributed to the fact that RiOMar form part of the land–ocean continuum. This continuum is characterized by more complex OC provenance, a dynamic sedimentary environment, and a less constrained carbon budget (Bianchi, 2011; Blair and Aller, 2012; Bauer et al., 2013; Najjar et al., 2018). Human activities and climate change have a pronounced effect on the influx of OC_{terr} and the marine sedimentary environment. These activities can influence the movement of OC deposited in the RiOMar, adding further complexity to the 'geochemical conundrum' (Canuel et al., 2012; Bauer et al., 2013; Regnier et al., 2013; Wang et al., 2020a). Therefore, further research is required to map processes influencing fate of OC_{terr} upon its entry into the RiOMar, including examining the sources of OC_{terr}, and defining the processes that affect its burial.

The East China Sea (ECS) is an ideal region for studying OC_{terr} cycling, because it is a typical RiOMar that receives high volumes of OC_{terr} via river inputs (Wu et al., 2018). The ECS has a great capacity to trap OC_{terr} because of its wide and shallow continental shelf (Deng et al., 2006; Hu et al., 2012). In addition, concentrated human activity in the river basin has led to a drastic reduction in sediment loads, which has substantially changed the source, composition, and flux of OC_{terr} entering the ECS (Bao et al., 2014; Li et al., 2015; Wu et al., 2018). The reduction in sediment loads has also affected the geomorphic stability of the ECS (Gao et al., 2019), triggering seabed erosion in the estuarine-inner shelf region, and changing OC dispersal and burial patterns (Wang et al., 2020a). These changes provide a unique opportunity to study the fate of OC_{terr} in RiOMar.

Several approaches have been used to examine the source, composition, distribution, transport, and burial of OC_{terr} in the estuarine-inner shelf region of the ECS. Bulk OC properties, including the C/N ratio and $\delta^{13}C$, are the most widely used proxies for examining source and composition of OC (Kao et al., 2003; Hu et al., 2012). Molecular biomarkers that are unique to terrestrial environments and diagenetically persistent provide alternative approach to track the fate of OC_{terr} from the continent to ocean margins. These include leaf wax, lignin phenols, and bacterial lipids (Eglinton and Hamilton, 1967; Hedges and Mann, 1979; Hopmans et al., 2004). Other relevant proxies have also been used extensively in the ECS to examine processes influencing the fate of OC_{terr} (Xing et al., 2011; Li et al., 2012; Yao et al., 2015). Contributions of terrestrial and marine OC into the system have been deduced based on the end-member mixing model (Yao et al., 2015), which also takes into account deposition fluxes (Wang et al., 2020a). Nevertheless, there are still areas for further study to improve our understanding of the fate of OC_{terr} in ECS. Several studies have only focused on a single index, providing results with a limited scope. However, studies with multi-index parameters, focused on research areas that were predominantly limited to the estuary, without revealing findings at the larger scale from the estuarine-inner shelf region of the ECS. As a typical source-to-sink (S2S) conveying system, the continent–river–coastal margin continuum dominates transport and burial of OC_{terr}. Therefore, attention should be paid to the transport of OC_{terr} in this context; and this approach requires a focus on the input river, namely, the Changjiang River (CJR, also known as the Yangtze River). Increasing human activity will likely have affected the fate of OC_{terr} in the CJR-ECS S2S conveying system.

The objectives of this study were to: (i) examine the composition of OC_{terr} in the ECS; (ii) provide a synoptic view of OC_{terr} distribution in the surficial sediments of the ECS, based on lipid biomarkers; (iii) evaluate geographic differences in the composition and degradation of OC_{terr} between 2006 and 2018; and (iv) explore the effects of human-induced changes to the catchment on the fate of OC_{terr} in the ECS by comparing our results with those of previous studies. This study builds on previous ECS research carried out at bulk and molecular levels (Hu et al., 2012; Zhu et al., 2013; Wang et al., 2020a, and references therein). Our main goal is to develop a more comprehensive conceptual model for ECS sediment in which the input, transport, and degradation of OC_{terr} can be qualitatively expressed in terms of diverse sub-categories.

2. BACKGROUND

The ECS is a typical RiOMar, primarily influenced by the CJR, which is the longest river in Europe and Asia. Historically, this river has discharged sediment loads of 478 Mt yr^{-1} (Mt: million ton) (Milliman and Farnsworth, 2011). However, this situation changed after the 1980s (Gao et al., 2018). There are > 50,000 reservoirs that have been constructed in the CJR river basin (Yang et al., 2011), which intercept sediment at rates of up to 453 Mt yr^{-1} (Gao et al., 2018). Sediment loads discharged into the ECS have decreased from 511 Mt yr^{-1} in 1956–1968, to 450 Mt yr^{-1} in 1968–1985, 340 Mt yr^{-1} in 1986–2002, 145 Mt yr^{-1} in 2003–2012 (following the construction of the Three Gorges Reservoir, TGR), to 118 Mt yr^{-1} in 2013–2015 (following construction of the Cascade dams) (Yang et al., 2018a). The Water and Soil Conservation Project, implemented in the 1980 s in the high-sediment-yield region of the upper CJR basin may also have resulted in an abrupt reduction in the sediment loads (Dai and Lu, 2014). The drastic reduction of the sediment loads has caused substantial changes in the sedimentary environment and the hydrodynamics of the ECS estuarine-inner shelf regions (Gao et al., 2017; Yang et al., 2018b; Wang et al., 2018). Reservoir interception of coarse-grained sediment from the upstream has induced channel erosion in the mid-downstream, substantially changing the composition of the sediment component reaching the ECS (Yang et al., 2014; Gao et al., 2018).

The Changjiang River Estuary (CRE) is located in the north of 30°N; a region characterized by surficial sediments that are mostly clayey silt. The sedimentation rate in the CRE gradually decreases from the near estuary to the front edge of the subaqueous delta (DeMaster et al., 1985). During winter, a portion of the Changjiang-derived sediments deposited in the CRE are carried southward by the Zhejiang–Fujian coastal current (ZFCC), forming the Zhejiang–Fujian coastal mud belt (ZFCMB) (Liu et al., 2007). The ZFCMB is in the Zhejiang–Fujian coastal area, south of the CRE, with a water depth of <60 m. This mud belt consists of silty mud, muddy silt, and other mixed deposits. The ZFCMB extends over 800 km southwards from the CRE, with a maximum thickness of 40 m seen at the 20–30 m isobath. The mud belt gradually thins toward both sides (Liu et al., 2010).

The estuarine-inner shelf areas of the ECS have three primary circulation systems, namely, the Changjiang diluted water (CDW), the ZFCC, and the Taiwan warm current (TWC) (Fig. 1a). The CDW is formed by freshwater from the CJR mixing with offshore water. It is characterized by low salinity and low density, forming a buoyant surface layer. During summer, this runoff first moves southeast and then expands northeastward toward Jeju Island (Chang et al., 2014). The ZFCC is in the Zhejiang–Fujian coastal area south of the CRE, is characterized by low salinity and a substantial variation in annual temperatures (Hu et al., 2001). In winter, strong northerly winds form a strong southward current. In contrast, in summer, the current is driven northward adjacent to the coast by southerly winds (Yuan and Hsueh, 2010). The TWC stems from the Taiwan Strait and is subsumed into the Kuroshio Current from northeastern Taiwan, which steadily advances northwards. The position of this current remains relatively steady, with little interannual variability.

3. MATERIALS AND METHODS

3.1. Sample collection

Spanning a stretch of approximately 4,000 km, 22 sites along the CJR mainstem and eight tributaries were sampled between Panzhihua (in Sichuan Province) and the CRE in the wet season in July–August 2018 (Fig. 1). One surface-water sample was collected at each of the eight largest tributaries (Yalong, Dadu, Min, Jialing, Wu, Han, Dongting, and Poyang) close to the confluence with the CJR, as well as at the CJR mainstem 10 km downstream from each major tributary confluence. There were 13 sites in the mainstem; with seven sites further upstream, three sites in the middle reaches of the river, and three sites further downstream, along with nine sites in the river tributaries. Water samples (100 L) were collected from each sampling site 0.5 m below the air–water surface using a metal bucket. The samples were filtered immediately after collection through pre-combusted (450 °C, 5 h) Whatman GF/F filters (nominal pore size: 0.7 μm) to obtain at least 15 g of suspended particulate matter (SPM) from each site. All the SPM samples were then stored at −20 °C until analysis.

All the surficial sediments were collected during three oceanographic cruises in March 2018 on the R/V *Kexue* 3; in March 2018 on the R/V *Xiangyanghong* 18; and in May 2018 on the R/V *Suruyu* 08,327 (Fig. 1b). For the first cruise, the sampling areas comprised the CRE. The second cruise targeted sampling sites on the inner and outer shelf of the ECS, along the shore of the Zhejiang and Fujian provinces. During the third cruise, several surficial sediment samples were collected from the ZFCMB, along the sediment dispersal system (approximately 30–60 m). A total of 126 surficial sediments (0–2 cm) were collected from the estuarine-inner shelf region of the ECS using a box corer. All the sediment samples were stored frozen (−20 °C) until analysis.

3.2. Sedimentological parameters

The grain size was analyzed as described by Wang et al. (2018). All the samples were treated with an H_2O_2 solution (10%) to remove organic matter, prior to the samples being immersed in sodium metaphosphate for 24 h. The grain size was measured using a laser diffraction particle size analyzer (Mastersizer 2000, Malven Instruments Ltd., UK). For each five samples, the test was repeated for one sample three times, with a measurement error of <3%.

The specific surface area (SSA) of the sediments was determined using nitrogen adsorption following the method described by Waterson and Canuel (2008). An aliquot of sediment (approximately 1 g) was freeze-dried and then heated at 350 °C for 12 h to remove the OC. The sample was then degassed for 0.5 h on an automatic nitrogen adsorption surface area analyzer (BSD-PS4, Beishide Instrument-ST Co., Ltd., China) at 200 °C to remove the water content, before being measured using the five-point Brunauer–Emmett–Teller method. The analytical precision of this measurement is better than ±1%, according to the triplicate measurement of one sample in each five sample.

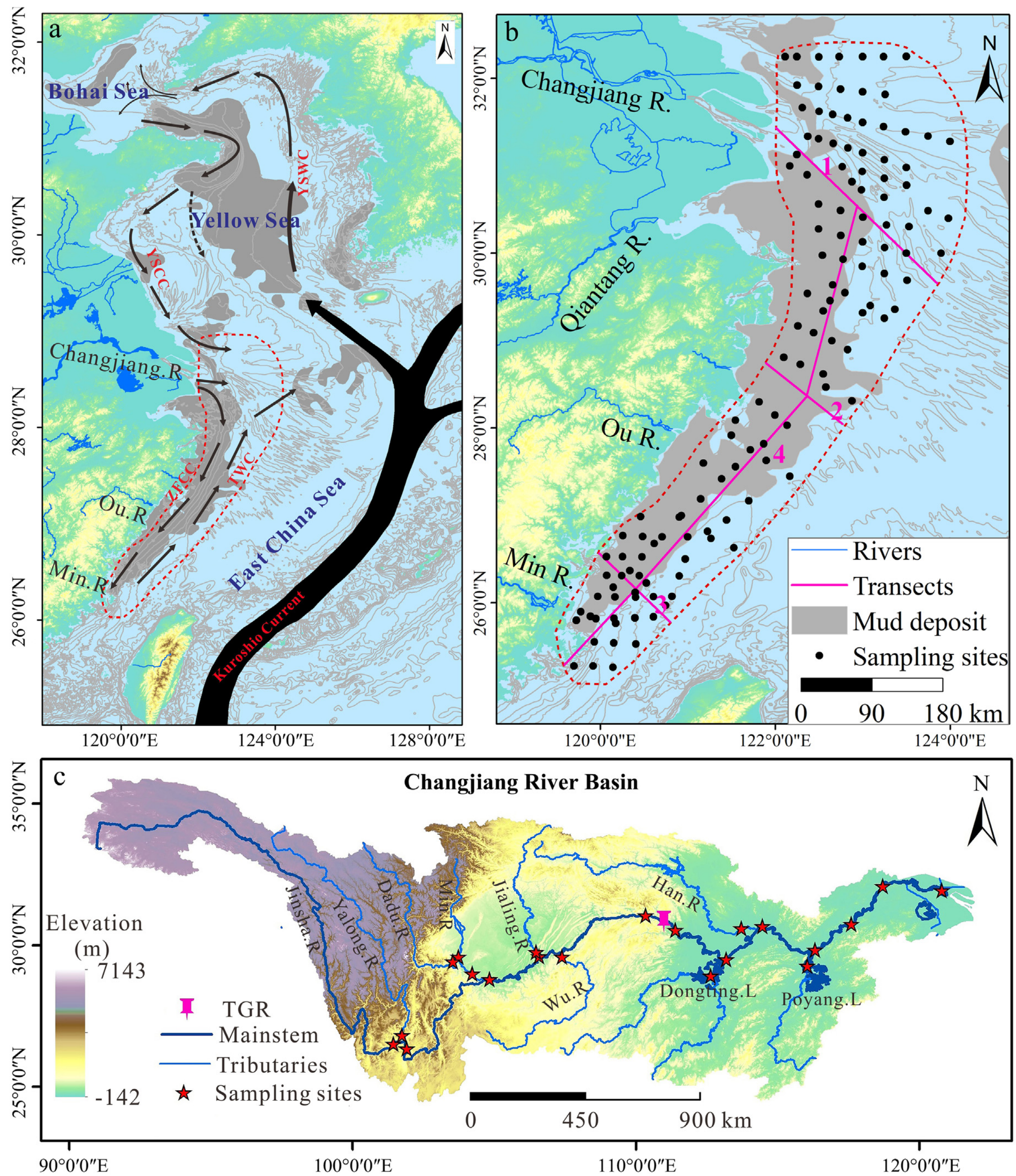

Fig. 1. Overview of the Changjiang-East China Sea system; (a) major oceanic currents including the Changjiang-diluted water (CDW), the Zhejiang-Fujian coastal current (ZFCC), the Taiwan warm current (TWC), the Yellow Sea coastal current (YSCC), the Yellow Sea warm current (YSWC), and the Kuroshio current. (b) Sampling sites in the estuarine-inner shelf areas of the ECS, with the red dotted line delineating the study area and gray areas representing mud deposits; and (c) the Changjiang River basin,★ are the sampling stations, ◆ is the Three Gorges Reservoir (TGR). CRE: the Changjiang River Estuary, ZFCMB: the Zhejiang-Fujian coastal mud belt. (For interpretation of the references to colour in this figure legend, the reader is referred to the web version of this article.)

3.3. Bulk measurements

All the SPM and the surficial sediment samples were analyzed for total organic carbon (TOC) and stable isotopes, following the methods described by Xing et al. (2011) and Hu et al. (2012). The freeze-dried and homogenized samples were decalcified by being reacted with 4 N HCl for 24 h, and then rinsed several times with deionized water to neutralize them. A Thermo Flash 2000 elemental analyzer interfaced with a MAT-253 isotope ratio mass spectrometer was used to determine the TOC content and stable isotopes. The precision of the TOC determination for the sediment samples was better than ± 0.02 wt% (n = 15). The value of $\delta^{13}C$ was reported in units per million (‰) as follows:

$$\delta^{13}C = \left(R_{sample}/R_{standard} - 1\right) \times 1000 \quad (1)$$

where R_{sample} and $R_{standard}$ are the ratios of $^{13}C/^{12}C$ for the sample and standard, respectively. The $\delta^{13}C$ values were reported using standard notation relative to the V-PDB (Vienna Pee Dee Belemnite) standard. The analytical precision was better than ± 0.1‰ based on replicate measurements (n = 15).

3.4. Lipid extraction and analysis

A total of 22 SPM samples and 145 surficial sediment samples were freeze-dried and homogenized for biomarker analysis. The biomarkers were analyzed as described by Guo et al. (2019a). Approximately 2 g from the SPM sample and 5 g for the surficial sediment sample were placed in a 50 ml Teflon tube, and the internal standards of nC_{36} alkane and C_{46} glycerol trialkyl glycerol tetraethers were added to each sample. The samples were then sequentially ultrasonically extracted thrice with methanol, thrice with a 1:1 v/v mixture of dichloromethane and methanol, and then thrice only with dichloromethane. Each extract was then saponified by adding 6% KOH in methanol to obtain a neutral lipid fraction. The neutral fraction was then passed through a silica gel chromatography column and eluted with hexane and methanol to separate the *n*-alkanes and the GDGTs.

The *n*-alkanes were identified and quantified using a HP 6890 gas chromatograph with a flame ionization detector and a DB-5 capillary column (50 m × 0.32 mm × 0.25 µm film thickness). Helium was used as the carrier gas. The peak area of each alkane was integrated and compared with the appropriate peak area for the relevant internal standard to quantify the content.

The GDGT analysis was performed using a high-performance liquid chromatography-mass spectrometry instrument (HPLC-MS; Agilent 1200 6410 triple quadrupole). The procedures described by Hopmans et al. (2004) and Schouten et al. (2007) were applied. Separation was achieved with a Prevail Cyano column (2.1 × 150 mm, 3 µm diameter; Grace, USA) and the temperature was maintained at 30 °C. The GDGTs were eluted isocratically with 99% hexane and 1% propanol for 5 min, followed by a linear gradient to 1.8% propanol for 45 min. The flow rate was 0.2 ml min^{-1}. Detection was achieved using APCI via selected ion monitoring (SIM) of $[M + H]^+$ ions (in MS1). GDGT indices with Arabic or Roman numerals corresponding to the structures shown in Fig. S1.

3.5. Molecular biomarker proxies

The odd-to-even carbon preference index (CPI) for long-chain *n*-alkanes is commonly used as an indicator of the thermal maturity of OC, which is typically used to indicate OC sources. The CPI index was calculated according to Bray and Evans (1961), as follows:

$$CPI_{25-33} = \frac{1}{2}\left(\frac{C_{25}+C_{27}+C_{29}+C_{31}+C_{33}}{C_{24}+C_{26}+C_{28}+C_{30}+C_{32}} + \frac{C_{25}+C_{27}+C_{29}+C_{31}+C_{33}}{C_{26}+C_{28}+C_{30}+C_{32}+C_{34}}\right) \quad (2)$$

The Branched and Isoprenoid Tetraether (BIT) index was calculated according to Hopmans et al. (2004) and is based on the relative abundance of branched glycerol dialkyl glycerol tetraethers (brGDGTs, Sinninghe Damsté et al., 2000) versus structurally related isoprenoid GDGTs (isoGDGTs, Sinninghe Damsté et al., 2002b). The BIT index was calculated as follows:

$$BIT = \frac{[(Ia) + (IIa) + (IIIa) + (IIa') + (IIIa')]}{[(Ia) + (IIa) + (IIIa) + (IIa') + (IIIa') + (Cren)]} \quad (3)$$

The #Rings$_{tetra}$ parameter was used to identify the source of the brGDGTs, and was defined as follows (Sinninghe Damsté, 2016):

$$\#Rings_{tetra} = \frac{(Ib + 2 \times Ic)}{(Ia + Ib + Ic)} \quad (4)$$

The roman numerals in Eq. (3) and (4) refer to the concentrations of GDGTs whose structures are shown in the Appendix: Ia, Ib, and Ic are basic tetramethylated brGDGTs; IIa and IIIa are 5-methyl brGDGTs, IIa′ and IIIa′ are 6-methyl brGDGTs; and IV is the isoGDGT "crenarchaeol," which is a specific membrane-spanning lipid from Thaumarchaeota (Sinninghe Damsté et al., 2002b).

3.6. Data collection

The *n*-alkanes concentration of sediments (n = 71) from the study area in 2006 were collected from Hu et al. (2012). The relative abundances of individual GDGT of sediments (n = 39) in 2006 were provided by Zhu et al. (2013). The datasets of bulk OC properties (TOC content, C/N ratio, and $\delta^{13}C$) and sedimentological parameters (grain size, components) were collected based on Hu et al. (2012) and Wang et al. (2020a).

3.7. Statistics

SPSS software (version 22.0; SPSS Institute, USA) was used for statistical analyses. The mean and standard deviation were first calculated. Statistical differences of sediment grain sizes/components, bulk OC properties, and biomarker properties for 2006 and 2018 were examined with Mann - Whitney *U* test, because these parameters were not normal distribution. Finally, a Pearson correlation matrix was created using the OC characteristics and sediment grain sizes from each station.

4. RESULTS

4.1. Bulk OC properties

4.1.1. Suspended particulate matter (SPM) in the Changjiang River (CJR)

The TOC content of river SPM ranged from 0.85% to 3.62% in the mainstem and the tributaries, with the lowest value occurring at Jialing River (an upstream tributary). The highest value was recorded at the final sampling site near the estuary (Table 1). The C/N ratio of SPM in the CJR basin varied from 6.18 to 17.25, with the lowest and highest values being recorded at the Jialing and Jinsha Rivers, respectively (Table 1). The $\delta^{13}C$ values of the SPM in the mainstem ranged from −27.54‰ to −24.95‰, which was in the range of −32.39‰ to −24.50‰ in the tributaries (Table 1).

4.1.2. Surficial sediments in the East China Sea (ECS)

The TOC content in the surficial sediments in 2006 and 2018 varied from 0.20% to 0.72% and 0.10% to 0.52% respectively (Fig. 2a, d), with mean values of 0.45 ± 0.21% and 0.35 ± 0.18% (mean ± standard deviation). The C/N ratio of the surficial sediments ranged from 1.1 to 10.9 in 2018, with a mean value of 6.8 ± 1.3. In 2006, the values were in the range of 6.0 – 11.1 (Fig. 2b, e), with a mean value of 8.4 ± 1.7. The $\delta^{13}C$ values in 2018 for the surficial sediments ranged from −23.80‰ to −20.45‰ (Fig. 2c), with a mean value of −22.30 ± 0.63‰. In 2006, the $\delta^{13}C$ value varied from −23.40‰ to −21.40‰ (Fig. 2f), with a mean value of −22.20 ± 0.40‰.

4.2. Biomarkers

4.2.1. SPM in the CJR

The distribution of *n*-alkanes in most of the river SPM samples ranged from nC_{14} to nC_{36}, with a dominance of long-chain *n*-alkanes ($nC_{25\text{-}33}$ alkanes; Table S1). The concentration of $nC_{14–36}$ alkanes was in the range of 95.57–738.62 μg g TOC^{-1}, with the highest value recorded at TGR (Table 1). The concentration of the $nC_{14–36}$ alkanes in the tributaries ranged from 208.54 to 1211.28 μg g TOC^{-1}, with the highest values occurring in the two largest freshwater lakes (Table 1). The concentration of $nC_{25–33}$ alkanes in the mainstem had a similar variation trend with $nC_{14–36}$ alkanes ranging from 62.35 to 212.61 μg g TOC^{-1} (Table 1). The concentration of the $nC_{25–33}$ alkanes in the tributaries ranged from 120.71 to 964.30 μg g TOC^{-1}, with the highest value occurring at Dongting Lake. The $CPI_{25–33}$ values in the mainstem ranged from 1.35 to 6.61, and the values in the tributaries ranged from 1.65 to 7.09, with the highest value also being recorded at Dongting Lake (Table 1).

The concentrations of the brGDGTs in the river SPM varied between 7.50 and 24.37 μg g TOC^{-1} in the mainstem, with the brGDGT concentrations in the tributaries ranging from 5.31 to 20.37 μg g TOC^{-1} (Table 1). The most abundant brGDGT in the river SPM was brGDGT Ia (20–67%), followed by brGDGT IIa (11–20%), and brGDGT IIa′ (10–22%). The concentrations of isoGDGTs in the river SPM ranged from 3.21 to 33.40 μg g TOC^{-1} in the mainstem, which showed a consistent trend with the brGDGTs (Table 1). The isoGDGT concentrations in the river SPM in the tributaries ranged from 2.30 to 111.54 μg g TOC^{-1}, and the concentrations in the two largest freshwater lakes were relatively low (Table 1). The distribution of the isoGDGTs was dominated by GDGT-0 (34–92%) and crenarchaeol, representing 5–55% of all isoGDGTs. The GDGT-0 to crenarchaeol ratio in the river SPM varied from 0.63 to 18.09, with a mean value of 3.93 ± 3.52. The BIT values of the river SPM in the mainstem varied from 0.74 to 0.94 (excluding extreme value in the Jialing River), with an average of 0.86 ± 0.05. The mainstem BIT values exhibited an upstream to midstream decreasing trend, but an increasing trend from midstream to downstream (Table 1). The BIT values of the river SPM in the tributaries ranged from 0.25 to 0.94. The $\#Rings_{tetra}$ index of the river SPM ranged from 0.09 to 0.48, with a mean value of 0.33 ± 0.11. The GDGTs data are listed in Table S2.

4.2.2. Surficial sediments in the East China Sea (ECS)

The concentration of $nC_{14–36}$ alkanes in 2018 in the surficial sediments ranged from 32.9 to 1,660.6 ng g^{-1} (Fig. 3a), with a mean value of 467.5 ± 266.2 ng g^{-1} (TOC normalized $nC_{14–36}$ alkanes ranged from 3.62 to 709.01 μg g TOC^{-1}, with a mean value of 111.14 ± 85.71 μg g TOC^{-1}). In 2006, the concentration of $nC_{14–36}$ alkanes ranged from 440 to 4310 ng g^{-1} (Fig. 3d), with a mean value of 2314 ± 512 ng g^{-1} (ranging from 147 to 757 μg g TOC^{-1} with a mean value of 430 ± 115 μg g TOC^{-1}). Additionally, the 2006 results exhibited a clear dividing line near 29° 30′ N, separating the study area into two north and south regions (Fig. 3). In 2006, the concentration of $nC_{25\text{-}33}$ alkanes ranged from 135 to 2786 ng g^{-1}; with a mean value of 1503 ± 613 ng g^{-1} (TOC normalized $nC_{25\text{-}33}$ alkanes abundance ranged from 74.8 to 410.6 μg g TOC^{-1}, with a mean value of 261.0 ± 84.3 μg g TOC^{-1}). In 2018 the $nC_{25\text{-}33}$ alkanes concentration ranged from 11 to 747 ng g^{-1}, with a mean value of 282 ± 167 ng g^{-1} (TOC normalized $nC_{25\text{-}33}$ alkanes abundance ranged from 8.8 to 170.0 μg g TOC^{-1}, with a mean value of 61.2 ± 29.8 μg g TOC^{-1}). All the *n*-alkanes data is listed in the Table S3.

The concentrations of brGDGTs and isoGDGTs in surficial sediments collected in 2018 are shown in Table S4 and Fig. S2; and their relative abundances are presented in Fig. S3. The brGDGT concentration of surficial sediments varied between 1.20 μg g TOC^{-1} and 246.56 μg g TOC^{-1}, with a mean value of 28.77 ± 24.24 μg g TOC^{-1} (Fig. S2); these trends show a high variability. The brGDGTs in surficial sediments was dominated by tetramethylated brGDGTs, ranging from 37% to 61%, with an average of 49 ± 5%. The proportion of 5-methyl and 6-methyl brGDGTs is the same, at 18–30% and 18–40%, respectively, with mean values of 24 ± 2% and 27 ± 4%. The $\#Rings_{tetra}$ index of the surficial sediments during 2018 varied from 0.40 to 1.07, with a mean of 0.70 ± 0.16 (Fig. 4a). The BIT values in 2018 ranged from 0.01 to 0.42, with a mean of 0.06 ± 0.05; the highest values were in the coastal and estuarine sediments (Fig. 4c). The isoGDGT concentrations of surficial sediments is in the range of 22.13–2687.77 μg g TOC^{-1}, with a mean value of 604.99 ± 428.79 μg g TOC^{-1} (Fig. S2). The high isoGDGT concentrations mainly occurred far from coast, opposing the trend seen in brGDGTs (Fig. S2). Cernarchaeol is more abundant in surficial sediments, forming 5–67% of the isoGDGT concentration. The GDGT-0 also

Table 1
Sedimentological characteristics, bulk OC properties, and abundance of the $nC_{14–36}$ alkanes, $nC_{25–33}$ alkanes, and brGDGT and isoGDGT compounds in the SPM. The calculated $CPI_{25–33}$ [Eq. (2)] and BIT index [Eq. (3)] are also reported.

	Stations	Lon (°)	Lat (°)	$\delta^{13}C$ (‰)	TOC (%)	C/N	$nC_{14–36}$ alkanes ($\mu g\ g\ TOC^{-1}$)	$nC_{25–33}$ alkanes ($\mu g\ g\ TOC^{-1}$)	$CPI_{25–33}$	brGDGT-I[a] ($\mu g\ g\ TOC^{-1}$)	brGDGT-II[b] ($\mu g\ g\ TOC^{-1}$)	brGDGT-III[c] ($\mu g\ g\ TOC^{-1}$)	ΣbrGDGTs ($\mu g\ g\ TOC^{-1}$)	ΣisoGDGTs ($\mu g\ g\ TOC^{-1}$)	BIT
	Mainstem														
	Jinsha River	101.80	26.60	25.25	1.61	17.25	262.98	167.00	6.61	3.23	3.21	1.06	7.50	3.21	0.88
	Panzhihua	101.82	26.61	24.95	1.57	14.82	259.95	175.88	6.32	3.91	3.20	0.90	8.00	4.06	0.85
Upstream	Yibin	104.67	28.77	25.32	1.12	9.72	323.15	156.86	4.40	3.50	5.00	1.54	10.04	6.14	0.87
	Chongqing	106.60	29.62	26.23	1.72	9.99	305.68	178.95	5.33	5.12	6.49	2.03	13.65	7.46	0.86
	Fuling	107.42	29.75	26.10	1.91	10.22	95.57	62.35	5.32	4.15	5.49	1.73	11.37	6.20	0.88
	TGR	110.99	30.84	25.47	1.47	10.43	738.62	212.61	1.35	5.68	7.07	2.10	14.85	13.92	0.81
	Yichang	111.29	30.73	25.40	1.13	8.63	387.71	180.81	2.97	8.95	11.81	3.55	24.31	21.30	0.84
	Yueyang	113.19	29.48	26.85	1.53	8.52	396.11	157.51	2.97	4.68	6.10	1.63	12.41	8.66	0.81
Midstream	Wuhan	114.55	30.65	25.87	1.57	8.58	365.55	140.11	3.54	6.09	8.10	2.12	16.31	12.91	0.79
	Jiujiang	116.30	29.80	25.10	1.18	6.97	471.47	197.73	2.30	6.70	8.18	1.78	16.66	12.65	0.80
	Datong	117.64	30.77	25.75	2.09	10.45	219.02	80.66	2.69	5.93	8.01	1.73	15.67	10.08	0.83
Downstream	Nanjing	118.66	31.97	25.35	1.10	9.00	349.76	112.32	1.96	6.73	8.48	1.74	16.95	10.18	0.85
	Xuliujing	120.99	31.76	27.54	3.62	6.61	3675.49	1536.62	1.30	7.72	9.23	1.71	18.66	33.42	0.91
	Tributary														
	Yalong River	101.81	26.61	24.50	1.34	11.24	338.33	204.81	6.02	3.34	3.02	1.06	7.42	3.55	0.86
	Min River	103.76	29.63	25.06	1.86	8.67	434.47	149.11	1.65	8.51	9.37	2.48	20.36	26.99	0.84
Upstream	Dadu River	103.73	29.56	25.30	1.24	8.53	315.74	156.22	3.90	8.40	8.88	2.50	19.79	11.71	0.88
	Min River Ⅱ	104.61	28.79	25.45	1.55	10.00	170.62	85.21	4.61	3.63	5.48	2.10	11.22	6.16	0.91
	Jialing River	106.55	29.57	25.83	0.85	6.18	303.43	120.71	3.05	7.77	9.78	2.46	20.01	111.54	0.25
	Wu River	107.42	29.71	25.44	0.97	6.39	208.54	127.67	4.97	6.40	9.68	2.89	18.97	16.64	0.74
	Han River	114.21	30.59	25.81	2.10	10.57	281.20	71.37	3.04	5.41	8.72	2.13	16.26	7.13	0.90
Mid-downstream	Dongting Lake	113.08	29.29	28.25	1.72	7.78	1211.28	964.30	7.09	3.25	1.82	0.24	5.31	2.30	0.94
	Poyang Lake	116.21	29.73	32.39	2.21	7.36	470.26	96.17	2.77	5.37	1.90	0.19	7.47	2.31	0.94

Note:
[a] GDGT-I = GDGT-Ia + GDGT-Ib + GDGT-Ic.
[b] GDGT-II = GDGT-IIa + GDGT-IIa′ + GDGT-IIb + GDGT-IIb′ + GDGT-IIc + GDGT-IIc′.
[c] GDGT-III = GDGT-IIIa + GDGT-IIIa′.

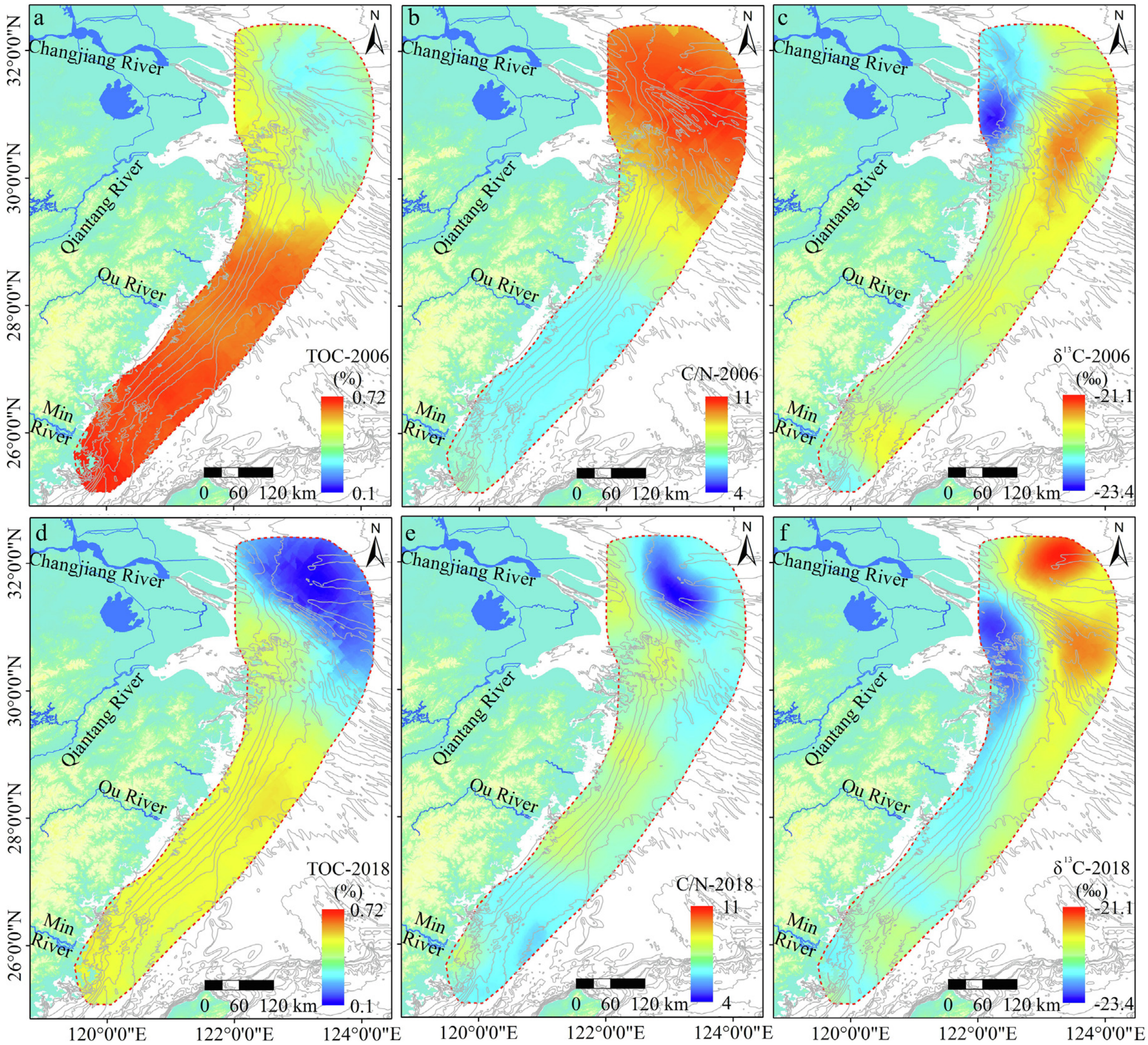

Fig. 2. Distribution patterns of bulk OC properties in the surficial sediments from the estuarine-inner shelf areas of the ECS in 2006 (upper row) and 2018 (lower row): (a, d) TOC content, (b, e) C/N ratio, (c, f) δ^{13}C value.

has high abundance in isoGDGTs, and its relative abundance varied from 18% to 90%, with a mean value of 28 ± 0.8%. The ratio between GDGT-0 and cernarchaeol varied from 0.34 to 0.62, with a mean value of 0.44 ± 0.05 (Fig. 4b).

4.3. Surficial sediment grain size in the ECS

The grain size distribution in the surficial sediment was extensively explored in our previous study (Wang et al., 2020b). In 2018, the sediment grain size ranged from 0 to 7.4 Φ, with a mean value of 4.4 ± 2.1 Φ. In 2006, it was in the range of 2.5–7.3 Φ, with a mean value of 6.4 ± 1.2 Φ (Fig. S4a, e). The datasets from 1982 were obtained from published literature; and they showed that the grain size of surficial sediments in the CRE ranged from 3.9 to 8.7 Φ, with a mean of 7.0 Φ (Yang et al., 2018b). The grain sizes in the ZMCMB ranged from 6.4 to 7.2 Φ, with a mean of 7.0 Φ (Gao et al., 2019). The datasets from 2014 were also collected, and they revealed a surficial sediment grain size ranging from 1.9 to 8.7 Φ, with a mean value of 5.6 ± 1.2 Φ (Gao et al., 2019).

The spatial distribution patterns of clay, silt, and sand in the surficial sediment were also delineated in the current study. In 2018, the clay in the surficial sediments ranged from 0 to 13.5%, with a mean value of 3.7 ± 2.8%, which is substantially lower than that of 2006 (ranging from 17.2 to 30.3% with a mean value of 25.2 ± 2.1%, Mann - Whitney U test, $P < 0.001$) (Fig. S4b, f). In contrast, the sand component increased from 3.5 ± 3.1% in 2006 to 31 ± 25.1% in 2018 (Mann - Whitney U test, $P < 0.001$), especially for the CRE, due to erosion (Fig. S4d, h). In 2018, the silt component ranged from 9.8 to 84.5% with a mean value of 70.2 ± 22.5%, which is consistent with that of 2006 (ranging from 32.2 to 73.4% with a mean value of 65.3 ± 9.4%) (Fig. S4c, g).

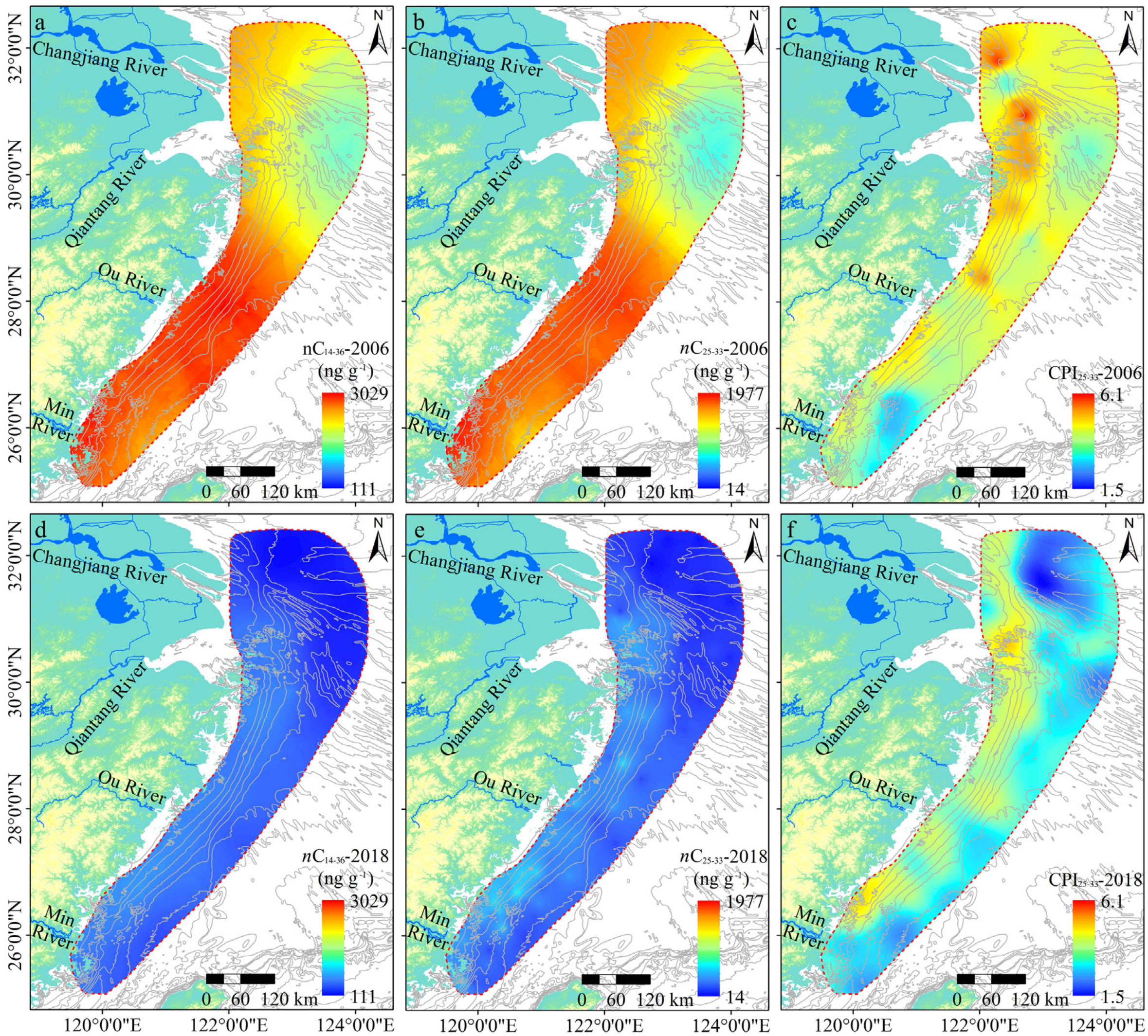

Fig. 3. Distribution patterns of *n*-alkanes abundances in the surficial sediments from the estuarine-inner shelf areas of the ECS in 2006 (upper row) and 2018 (lower row): (a, d) $nC_{14–36}$ alkanes, (b, e) $nC_{25\text{-}33}$ alkanes, (c, f) $CPI_{25–33}$.

5. DISCUSSION

5.1. Responses of the sedimentary environment to the reduction in sediment loads

The surficial sediments in the estuarine-inner shelf area of the ECS in 1982 were mainly fine-grained particles, which is consistent with that of 2006. In 2014, the surficial sediment grain size exhibited a certain extent coarsening, and in 2018, the mean value of the surficial sediment grain size was coarser by about 2 Φ than in 2006, suggesting a substantial coarsening trend across the study area (Fig. S4). The mean grain size values in the time series for this study show a coarsening of the surficial sediments after 2006, which is consistent with reservoir construction. Therefore, the seabed in the study area having shifted from accretion to erosion due to reduction of fluvial sediment loads, and similar situation also occurred in the Yellow River estuary, Red River estuary, and Mississippi River subaqueous delta (Maloney et al., 2018; Dac Ve et al., 2021; Liu et al., 2022).

The clay and sand of surficial sediments in 2018 changed substantially both in spatial distribution and contents than that in 2006. The silt content of the sediments was similar in 2006 and 2018, but the spatial distribution pattern changed substantially. This was relatively homogeneous over the whole region in 2006, but then changed to being high for the ZMCMB and low for the CRE (Fig. S4). After the TGR impoundment, sediment loads being discharged from the CJR decreased by approximately 150 Mt yr^{-1}. Climate change and changes in land-use have been highlighted as two main causative agents in reduction of sediment discharged into the ocean margins (Zhao et al., 2015; Guo et al., 2019b); but previous studies have suggested that climate change was less important (Dai and Lu, 2014; Yang et al., 2015). Zhao et al. (2015) suggested that climate change directly responsible for <10% of the sediment load reduction in

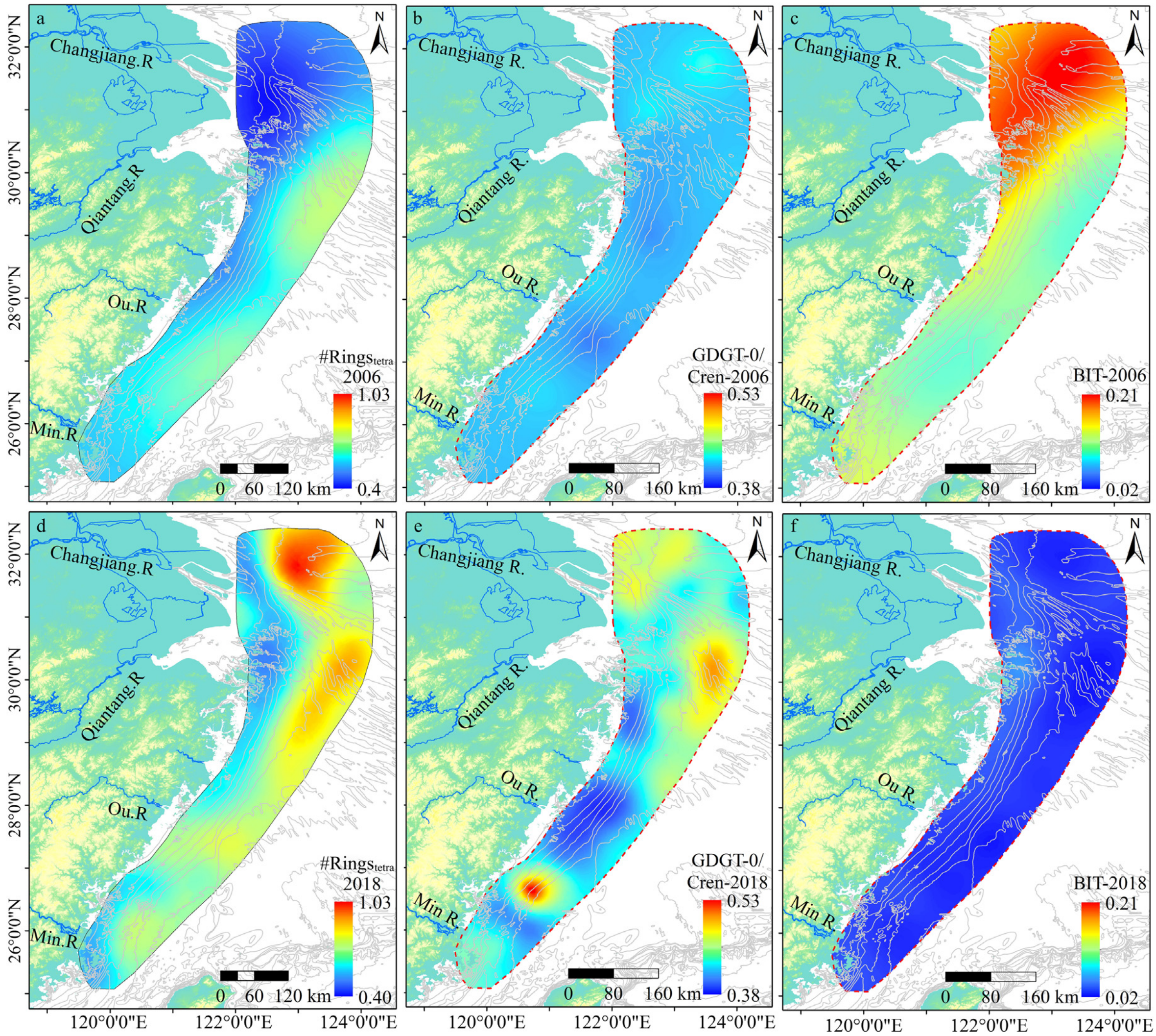

Fig. 4. Distribution patterns of GDGT-derived indices in the surficial sediments from the estuarine-inner shelf areas of the ECS in 2006 (upper row) and 2018 (lower row): (a, d) #Rings$_{tetra}$, (b, e) GDGT-0/Crenarchaeol; (c, f) BIT value.

CJR basin during the 2000 s. Land-use change affected sediment load mainly before the 2000 s, because of large-scale reforestation measures in regions with a high sediment yield (Dai and Lu, 2014). Therefore, reservoir interception is likely the dominant factor reducing sediment flux in the 21st Century. The current Changjiang-derived sediment load is substantially lower than the critical value of approximately 300 Mt yr^{-1}; this is the threshold value of sediment load needed to maintain the stability of the sedimentary environment (Gao and Wang, 2008; Yang et al., 2011). A drop below this threshold causes a water discharge with low sediment concentration, which is characterized by high carrying capacities. Therefore, larger amounts of fine-grained sediments, such as clay and silt, have been eroded and transported southward, with clay being transported to the outer shelf of the ECS. These variations in the sedimentary environment would likely influence the distribution and burial of sediment-associated terrestrial materials such as OC$_{terr}$ in the ECS.

5.2. Characterizing the OC properties in the CJR-ECS S2S conveying system

5.2.1. Trends in OC properties in the CJR basin

Although there was not trend in the TOC content of the river SPM from upstream to downstream ($r^2 = 0.01$, $P > 0.05$), the C/N ratio in the mainstem decreased from upstream to downstream ($r^2 = 0.78$, $P < 0.01$). The C/N ratio in the mainstream is higher than that of the northern tributaries (Table 1). This suggests that the contributions from the tributaries may be an important factor in influencing the C/N ratio of the mainstem. Wu et al. (2007) showed that the mean values of the C/N ratios of SPM from the up-midstream and downstream were 15.6 and 9.3, respectively, which is higher than the results of the current study (Table 1). Reservoir construction in the upstream tributaries would reduce the concentration of SPM in the mainstem leading to high transparency and increased phytoplankton productivity. This may also affect the C/N ratio of SPM, which is further illustrated by the lower C/N ratio in the downstream. Like TOC content, there was no trend in $\delta^{13}C$ values from upstream to downstream ($r^2 = 0.03$, $P > 0.05$). Lower $\delta^{13}C$ values for the SPM samples suggest that primary productivity is an important source of OC in the CJR. This is because phytoplankton growing in freshwater are typically deficient in δ13C ($\delta^{13}C = -30‰$ to $-40‰$) (Hedges et al., 1986; Tan and Edmond, 1993).

Prior to the construction of the TGR, the concentration of $nC_{14–36}$ alkanes increased downstream whereas we observed a decrease in *n*-alkanes after the TGR (Table 1). This change in *n*-alkane concentrations could be due to retention within the reservoir. The concentration of the $nC_{14–36}$ alkanes in the mid-downstream was higher than further upstream. The concentration of the $nC_{14–36}$ alkanes in the upstream tributaries was also lower than in the downstream tributaries (Table 1). As the main components of *n*-alkanes, the concentration of $nC_{25–33}$ alkanes in the CJR had a similar variation trend with the $nC_{14–36}$ alkanes. The $CPI_{25–33}$ values in the mainstem showed a strong decrease from upstream to downstream ($r^2 = 0.71$, $P < 0.01$). The $CPI_{25–33}$ of the SPM samples that were collected in 2001 was in the range of 0.91–3.39, with a mean value of 1.69 ± 0.63 (Qi et al., 2006), which is lower than the results of the current study (3.62 ± 1.74). The relative abundance of individual *n*-alkanes in the SPM samples revealed that the abundances of nC_{17} and nC_{18} alkanes were relatively high in short-chain *n*-alkanes after the impoundment of TGR, but this phenomenon was not observed in the samples collected in 2001 (Fig. S5). This indicated that phytoplankton productivity was also an important contributor of OC in the SPM samples, because the increased water transparency caused by reservoir interception.

5.2.2. Trends for OC properties in the surficial sediments from the ECS

The TOC content of the surficial sediments was lower in 2018 compared to 2006 (Fig. 2a, d). The surficial sediments in 2006 and 2018 displayed depleted-$\delta^{13}C$ values in the subaqueous delta, and enriched-$\delta^{13}C$ values east of 122°30′ (Fig. 2c, f). The sediments from the CRE and the ZMCMB had relative depleted-$\delta^{13}C$ values in 2018 compared with 2006, indicating an increase in the proportion of OC_{terr}. The C/N ratio of surficial sediments in 2018 decreased significantly (Mann - Whitney *U* test, $P < 0.001$), but with increased spatial variability compared to 2006 (Fig. 2b, e), indicating that the proportion of OC_{terr} in the surficial sediment decreased in the study area, especially for the CRE. However, the influx of OC_{terr} from the CJR to the ECS decreased by 70% after the TGR impoundment (Wang et al., 2020a). The likely provenances of the OC that were reflected by the $\delta^{13}C$ values and the C/N ratio are substantially different. Therefore, other indices should also be used to better determine the provenance of the OC.

The hydrocarbon fractions were dominated by a homologous series of $nC_{14–36}$ alkanes. These alkanes were characterized by a predominance of odd-numbered homologues, with the nC_{31} alkane being the most abundant (Table S3). The concentration of the $nC_{14–36}$ alkanes in the surficial sediments in 2018 significantly decreased from 2006 (Mann - Whitney *U* test, $P < 0.001$) for the ZMCMB, as well as the CRE (Fig. 3a, e). The spatial distribution pattern of the $nC_{14–36}$ alkanes was consistent with the TOC content and the sediment grain size, showing similar patterns in variability. The *n*-alkanes in the RiOMar usually show a bimodal patter; one in which the long-chain *n*-alkanes mainly stem from terrestrial higher vegetation and the short-chain *n*-alkanes mainly comes from marine phytoplankton (Eglinton and Hamilton, 1967; Belicka et al., 2002; Yunker et al., 2005). Data from 2006 showed that *n*-alkanes in the CRE had odd-over-even predominance, and the group with the highest abundance was the C_{31} *n*-alkanes (Table S3), indicating that the *n*-alkanes were strongly influenced by terrestrial input. With the extension of sampling stations further from the CRE and even to the southern part of the Zhejiang-Fujian coast, the proportion of short-chain *n*-alkanes gradually increased (Table S3), indicating that marine organic matter gradually increased. In 2018, the surficial sediments showed a preponderance for long-chain *n*-alkanes, especially for the CRE (Table S3), indicative of the increasing contributions of terrestrial inputs. Along the Zhejiang-Fujian coast, short- and long-chain *n*-alkanes had a bimodal distribution, but the proportion of short-chained *n*-alkanes increasing with distance far away from the CRE.

The alkyl lipid biomarker composition, including the ratio of terrestrial long-chain *n*-alkanes to the marine short-chain *n*-alkanes, offers a complementary interpretation of the relative contribution of terrestrial and marine sources (Karlsson et al., 2011). In 2006, the ratio ranged from 4.4 to 66 with a mean value of 20 ± 10, while in 2018 the ratio declined (ranging from 2 to 85, with a mean value of 13 ± 12; Mann - Whitney *U* test, $P < 0.001$), especially for the CRE (Fig. S6). The CPI_{25-33} value was also calculated (Fig. 3c, f); similarly, it showed a high value nearshore. The CPI_{25-33} values of the surficial sediments in 2006 ranged from 2.66 to 5.73, with a mean of 4.12 ± 0.57; those in 2018 ranged from 1.13 to 5.50, with a mean of 3.32 ± 0.93. This variation in CPI_{25-33} values indicates that the OC_{terr} in the study area had been subjected to degradation prior to or in 2018 (Mann - Whitney *U* test, $P < 0.001$). Additionally, we explored the variation in CPI_{25-33} values in each sub-region. The CPI_{25-33} values in the CRE decreased from 4.12 ± 0.57 in 2006 to 3.32 ± 0.93 in 2018 (Mann - Whitney *U* test, $P < 0.001$); those in the ZMCMB decreased from 3.87 ± 0.57 in 2006 to 3.35 ± 0.85 in 2018 (Mann - Whitney *U* test, $P < 0.001$). The CPI is a well-used marker for relative degradation state of *n*-alkanes (Fahl and Stein, 1997; Yamamoto et al., 2008), with living plants commonly have CPI values > 5, and during degradation this ratio decreases toward 1 (Rieley et al., 1991). Therefore, the degree of OC degradation in the CRE was higher than that in the ZMCMB, and this is consistent with the coarsening trend of sediment grain size.

GDGTs have recently raised substantial interest due to their potential as proxies to trace OC source, and brGDGTs were usually used as tracers for terrestrial input. Unfortunately, due to limitations in their analytical techniques, another group reported the relative abundance of

GDGTs in the study area (Zhu et al., 2011). Therefore, we further measured and compared the relative abundance of GDGTs in the surficial sediments collected in 2006 and 2018. The brGDGT abundances were highest in the estuary, followed by the nearshore, and were lowest offshore (Fig. S3a, c). This reveals the dispersal pattern of terrestrial materials after entering the ECS. The relative abundance of brGDGTs varied strongly among the surficial sediments in 2018, ranging from 1.2 to 37.4%, with a mean of 5.7 ± 5.3% (Fig. S3c). The brGDGT abundances in 2006 also showed high variability (Fig. S3a), ranging from 4.3 to 68.1%, with a mean of 17.7 ± 15.1%. Spatially, the relative abundance of brGDGTs in the CRE (mean values of 25.9 ± 18.2% in 2006 and 5.8 ± 5.4% in 2018) was higher than that in the ZMCMB (mean values of 8.9 ± 5.2% in 2006 and5.6 ± 5.4% in 2018) (Fig. S3a, c), indicating that riverine input can have a notable impact, especially for the CRE. However, the decreasing trend in brGDGTs over time was stronger for the CRE than for the ZMCMB. This is consistent with reservoir construction and its effect on riverine inputs to the estuary.

Previous studies have demonstrated that brGDGT distributions in marine sediment may be altered by in situ production (Peterse et al., 2009; Zell et al., 2014; Cao et al., 2020), which may affect the ability of using relative abundances to accurately determine the OC provenance. Thus, we explored whether a reduced riverine input would have an impact on the in situ production of GDGTs. Sinninghe Damsté (2016) suggested that the #Rings$_{tetra}$ index exhibits different responses in soil and marine sediment, with values < 0.7 in soil and reaching as high as 1 in coastal sediment. The #Rings$_{tetra}$ values of the surficial sediments in 2006 ranged from 0.31 to 0.96, with a mean of 0.62 ± 0.20, whereas they ranged from 0.40 to 1.07, with a mean of 0.70 ± 0.16, in 2018 (Fig. 4a, c). Spatially, the #Rings$_{tetra}$ values increased offshore, which is consistent with the findings of Cao et al. (2020). The relatively higher 2018 #Rings$_{tetra}$ values (Mann - Whitney U test, $P < 0.001$) indicate that brGDGTs in the surficial sediment could not be derived entirely from terrestrial inputs, and that in situ production could be an important source of brGDGTs. The relatively lower #Rings$_{tetra}$ values (0.33 ± 0.11) of SPM in the CJR also indicates that in situ production of brGDGTs occurred in the study area. Therefore, the source of brGDGTs in the study area could be altered, which may have an impact on interpretations of the OC source and sedimentary records using the relevant indices. As noted by Zell et al. (2004), brGDGT-derived indices should only be used for sedimentary environments that are under a strong riverine influence.

IsoGDGTs are membrane-spanning lipids mainly biosynthesized by Thaumarchaeota, which are abundant in marine environment. The distribution of isoGDGTs in the surficial sediment exhibited the opposite trend, with high abundances farther from the coast (Fig. S3b, d). The abundances of isoGDGTs in 2018 ranged from 62.6 to 98.8%, with a mean of 94.1 ± 5.2%, which were higher than those observed in 2006 (32.6–95.7%, mean of 82.5 ± 14.9%; Mann - Whitney U test, $P < 0.001$). The two most abundant isoGDGTs in the study area were GDGT-0 and crenarchaeol, while the relative abundances of the other components were minor and generally constant among the various depositional settings. The abundances of GDGT-0 and crenarchaeol in the surficial sediment in 2006 ranged from 11.3 to 28.8% (mean of 21.4 ± 3.7%) and from 17.6 to 60.7% (mean of 50.1 ± 9.4%), respectively, both of which were lower than those observed in 2018. Overall, the reduced riverine input corresponded to an increase in the relative abundance of isoGDGT.

To determine whether riverine isoGDGTs influenced the distribution of isoGDGTs in the marine sediment, the GDGT-0/crenarchaeol ratios were examined. GDGT-0 is a common archaeal membrane lipid with multiple sources, including methanogens and Thaumarchaeota (Sinninghe Damsté et al., 2002a; Schouten et al., 2013). In contrast, crenarchaeol appears to be predominantly produced by Thaumarchaeota (Sinninghe Damsté et al., 2002). The GDGT-0/crenarchaeol ratio of Thaumarchaeota depends on temperature, and typically ranges from 0.2 to 2 (Schouten et al., 2002). Blaga et al. (2009) suggested that ratios > 2 indicate a substantial methanogenic origin for GDGT-0. Therefore, this ratio is generally used to indicate different environmental conditions (river or coastal ocean) in the study area. In 2006, the GDGT-0/crenarchaeol ratio of the riverine SPM samples (1.96 ± 0.37) was higher than that of the surficial sediment in the ECS (0.34–0.64, mean of 0.43 ± 0.07; Fig. 4b), suggesting the presence of an additional GDGT-0 source in the basin and a low GDGT-0 contribution to the coastal ocean (Zhu et al., 2011; Zell et al., 2014). The ratio of the riverine SPM samples was 3.93 ± 3.52 in 2018, while that of the surficial sediment in the coastal ocean was 0.44 ± 0.05 (Fig. 4e). The relatively high ratio in 2018 may be related to eutrophication in the basin, as indicated by high methane emissions from the reservoirs (Liu et al., 2021; Deemer et al., 2016). Although the GDGT-0/crenarchaeol ratio of the riverine SPM increased considerably, that of the marine sediment remained unchanged between 2006 and 2018, indicating that decreased riverine inputs had a less impact on isoGDGT distributions in the marine sediment.

BIT is expressed as the amount of terrestrial brGDGTs relative to the amount of crenarchaeol (Eq. (3)) (Hopmans et al., 2004). BIT is useful for estimating the relative riverine inputs of terrestrial/soil OC to marine sediment, and returns a value of approximately 1 in a purely terrestrial setting and 0 in a marine setting (Hopmans et al., 2004; Weijers et al., 2006; Huguet et al., 2006). However, the BIT index has been shown to be selective, as BIT can be produced in situ in freshwater and marine environments (De Jonge et al., 2015; Sinninghe Damsté, 2016). In this study, the BIT index of the surficial sediment in 2018 had a mean of 0.06 ± 0.05, which was markedly lower than that in 2006 (0.19 ± 0.16). Spatially, the BIT index was homogeneous in the study area in 2018 (Fig. 4f), and only a few stations near the estuary exhibited relatively higher BIT values (BIT > 0.1). This is consistent with the findings of Cao et al. (2020). However, the distribution of the BIT index in 2006 exhibited spatial heterogeneity, with high values near the estuary and low values farther away. The BIT index of the stations near the estuary ranged from 0.66 to 0.96, with a mean value of 0.87 ± 0.11, which was approximately the same as the BIT index of the river SPM in this study (0.86 ± 0.05). >50% of the stations in estuaries and nearshore regions had BIT values > 0.1, indicating that a strong riverine influence corresponds to high BIT values in the study area. The drastic decrease in the BIT values in 2018 suggests that, although in situ production can impact brGDGTs, the impact of reduced riverine inputs cannot be ignored.

5.3. Controlling factors influencing changes in the fate of sediment OC

5.3.1. Alongshore or cross-shelf transport of OC_{terr}

The deposition and transport of terrestrial materials in the study area are predominantly controlled by the coastal currents, such as the CDW, ZMCC, and TWC, depicted in Fig. 1a. This circulation pattern leads to cross-shelf transport in the estuary and longshore transport in the Zhejiang–Fujian coastal zone. Cross-shelf transport often occurs between 28° N and 30° N, which is recognized as one of the principal channels for the transfer of coastal material to the open sea (Liu et al., 2015). The spatial distribution pattern of the TOC content in the surficial sediments was consistent with the circulation pattern, showing a pronounced decreasing trend from the estuary eastward to the open sea; and an increasing trend from the estuary southward to the Zhejiang–Fujian coast, as depicted in Fig. 2a, d. High TOC content was recorded near 28° N, which is consistent with the location of the cross-shelf penetrating fronts delineated by Yuan et al. (2005). As depicted in Fig. 3a, the concentration of the $nC_{14–36}$ alkanes (in 2018) in the surficial sediments from the estuarine-inner shelf region of the ECS was high nearshore, with lower values further from the coast. In 2006, the spatial distribution of the $nC_{14–36}$ alkanes showed a decreasing trend from the estuary (north of 29° 30′ N) eastward to offshore, while the inner shelf had a higher value (Fig. 3e). The concentration of the $nC_{14–36}$ alkanes in the surficial sediments from the estuary was lower than that from the Zhejiang–Fujian coast (Fig. 3a). The spatial distribution pattern of the $nC_{25–33}$ alkanes was similar to the $nC_{14–36}$ alkanes, with high values nearshore, and gradually decreasing towards the sea. The distribution pattern of the GDGTs in the surficial sediments revealed cross-shelf transport of OC_{terr} (Fig. 4). The concentration of the brGDGTs in the surficial sediments was high in the estuary and gradually lowered southward, which is consistent with the variation trend from nearshore to offshore (Fig. 4a, d). Meanwhile, the distribution pattern of isoGDGTs, which mainly originated from marine planktonic Thaumarchaeota, had opposite trends (Fig. 4b, e), i.e., increasing from nearshore to offshore.

To better understand the longshore or cross-shelf transport of OC_{terr}, the 'Profile Graph' tool in ArcGIS 10.2 was used to estimate continuous biomarker values along four transects. Transect 1 was in the estuary; transects 2 and 3 were along the Zhejiang and Fujian coasts; and transect 4 was from the estuary to the Taiwan Strait, as depicted in Fig. 1b. The variation patterns of the $nC_{14–36}$ alkanes, the $nC_{25–33}$ alkanes, the brGDGTs, and the $CPI_{25–33}$ in transects 1–3 revealed a uniform decreasing trend from the estuary and coastline to offshore, but the isoGDGTs showed a pronounced increase across these three transects (Fig. 5). Combined with the spatial distribution pattern and the cross-sectional variation trends for the target indices, we conclude that OC_{terr} is influenced by cross-shelf transport processes. In addition, in 2018 the distribution pattern for the target indices showed a notable tongue-shaped zone in the sediment grain size, the TOC content, $nC_{14–36}$ alkanes, and $nC_{25–33}$ alkanes, located between 28° N and 30° N, extending eastward to the boundary of the study area (Fig. S7). The tongue-shaped zones for these indices were not seen in 2006 (Fig. S7). In 2006, the surficial sediments south of 29° 30′ N were homogeneous fine-grained particles (>6.5 Φ) because of the abundant supplement of CJR-derived sediments. These variations confirmed the existence of cross-shelf transport processes in the ECS from the perspective of geochemistry, and this region can maintain a relatively stable sedimentary environment even with the reduced sediment supply.

Transect 4 is parallel to the axis of the mud deposits in the estuarine-inner shelf area of the ECS, and can better describe the variation trend of target indices in the direction of longshore transport. In 2006, the variation trends in the $nC_{14–36}$ and $nC_{25–33}$ alkanes showed a uniformly increasing trend, indicating higher values along the Zhejiang-Fujian coast (Fig. 5). However, this phenomenon did not occur in 2018, and there was a fluctuation in the distribution patterns (Fig. 5). Seabed erosion may be the main reason for these substantial fluctuations, leading to the widespread dispersion of fine-grained sediments and the associated OC. The variation trend in the brGDGTs first decreased and then increased, but the isoGDGTs had an opposite trend. The variation trend for the GDGTs in coastal transport was not consistent with that of *n*-alkanes, so there may be an additional input source in the southern region.

5.3.2. Influence of riverine input and hydrodynamics on the fate of OC_{terr}

Marginal seas are highly dynamic and heterogeneous, with spatially diverse sediment transport processes as well as OC inputs influencing the distribution and composition of sedimentary OC (Bao et al., 2016; Bianchi et al., 2018; Wang et al., 2020a). With continuous intensification of human activities in the basin, the output fluxes of the CJR-derived sediments and the associated OC, declined sharply (Gao et al., 2018, Wu et al., 2018). Li et al. (2015) estimated that dam building in the CJR basin has sequestered ~4.9 ± 1.9 Mt yr^{-1} of particulate OC since 2003, approximately 66% of the TOC burial flux to the ECS. Our previous study also demonstrated that approximately 84% of the POC from upstream was trapped in the TGR, resulting in the deposition flux of OC in the ECS being reduced by half (Wang et al., 2020a). Substantial changes in OC input will influence the distribution and composition of sedimentary OC in the study area.

Sedimentary environment in the study area have been demonstrated to be altered after 2006 due to reduction of riverine input (Wang et al., 2020b), which induced wide-

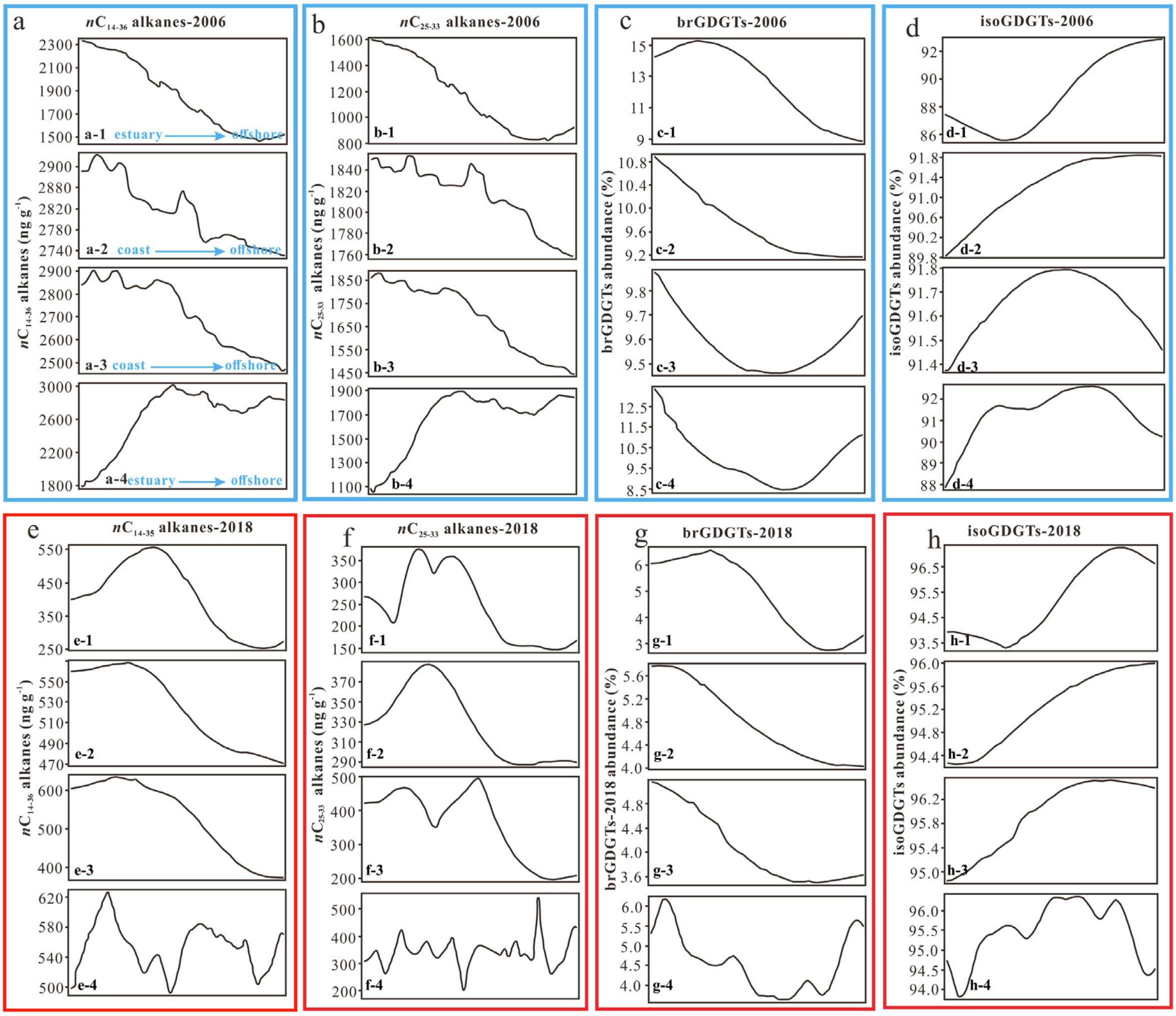

Fig. 5. Variation trends in estimate abundances of target biomarker in four typical transects from the estuarine-inner shelf areas of the ECS in 2006 (blue boxes) and 2018 (red boxes); a, e) nC_{14-36} alkanes; b, f) nC_{25-33} alkanes; c, g) brGDGTs; d, h) isoGDGTs. (For interpretation of the references to colour in this figure legend, the reader is referred to the web version of this article.)

spread sediment dispersal, but also affected the extent of degradation and the compositional characteristics of the associated OC (Bao et al., 2018; Bröder et al., 2018). To better understand the influence of sedimentary dynamic processes on the distribution of sedimentary OC in the study area, Spearman correlation analysis showed that the sediment grain size exhibited significant positive correlations with TOC content, nC_{14-36} alkanes, and nC_{25-33} alkanes both in 2006 and 2018 (Fig. 6). The correlations between sediment grain size and GDGTs proxies exhibited significant in 2018 and no significant in 2006 (Fig. 6). The significant correlations suggested that the fate of sedimentary OC will inevitably change due to wide dispersal of surficial sediments.

In addition, OC associated with different sedimentary grain-size fractions may be subject to different processes, particularly in continental shelf settings characterized by strong, dynamic, and diverse hydrodynamic gradients (McCave and Hall, 2006; Bao et al., 2019). To demonstrate the impact of hydraulic sorting on the sedimentary OC, a correlation analysis was also conducted between the target indices and the sediment components (clay, silt, and sand). The 2006 results showed that the clay and silt components were positively correlated with the TOC content, the nC_{14-36} alkanes, and the nC_{25-33} alkanes; and that the significance of silt was stronger than that of the clay component (Fig. 6). In 2018, the correlation results revealed a significant positive correlation between silt component and target indices, and a non-significant correlation between clay component and the target indices (Fig. 6). The substantial decrease in clay content could be an important controlling factor for OC transport, decreasing from 25.2 ± 2.1% in 2006 to 3.7 ± 2.8% in 2018, as depicted in Fig. 5. Therefore, the dispersal pattern of silt now exerts the strongest influence on the sedimentary OC in the study area. Meanwhile, as the main component of silt, the 'sortable silt' requires lower shear stress for erosion and return to suspension (McCave and Hall, 2006; Bao et al., 2018). Therefore, OC associated with silt may have a longer-distance transport process with potentially protracted

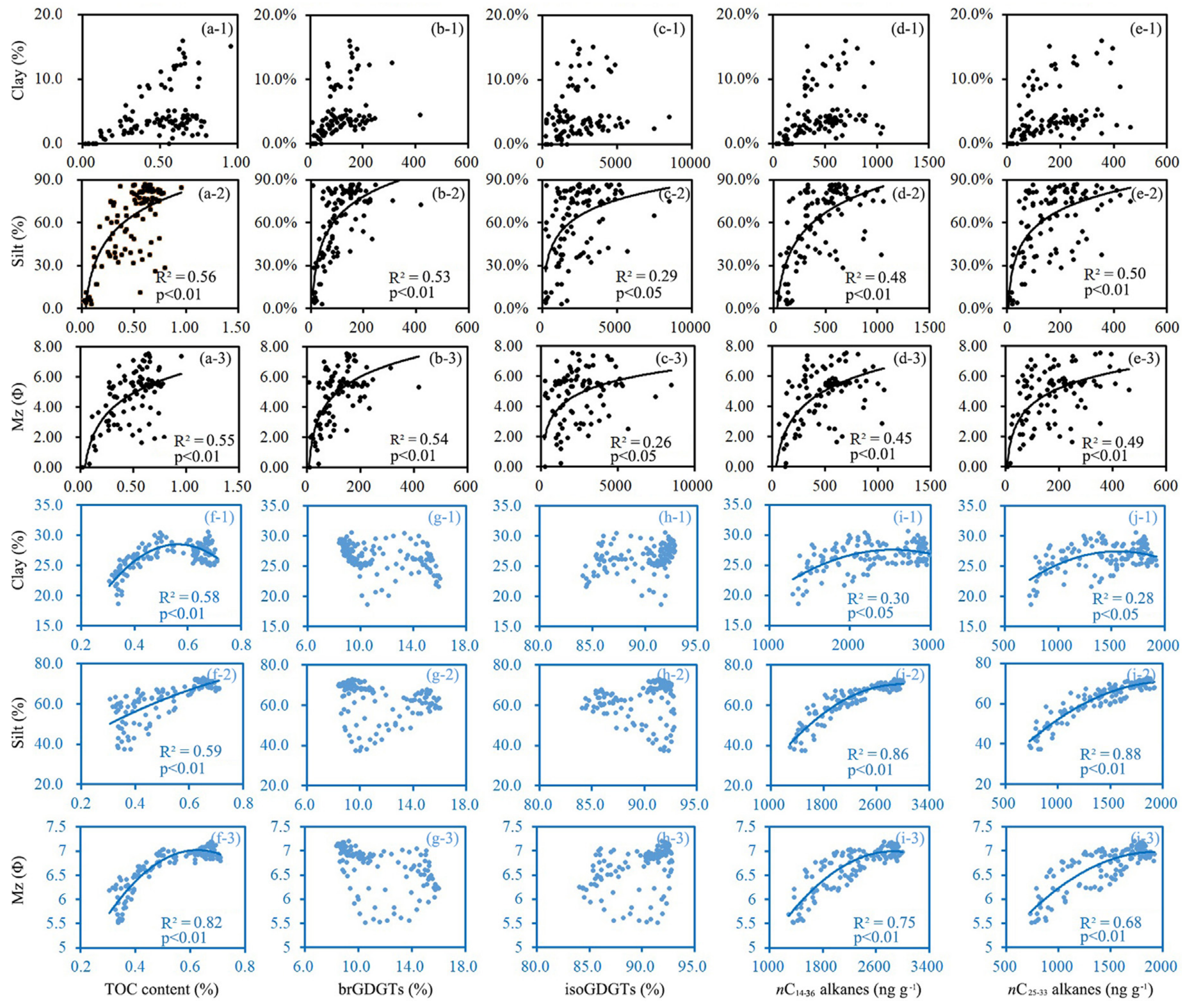

Fig. 6. Correlations between sedimentary properties (mean grain size, clay and silt) and TOC content/$nC_{14–36}$ alkanes/$nC_{25–33}$ alkanes in 2006 (blue boxes) and 2018 (black boxes); The solid line in the panels represents the curve fit. No line is shown when the fit was not statistically significant. (For interpretation of the references to colour in this figure legend, the reader is referred to the web version of this article.)

entrainment in resuspension-deposition loops (Ohkouchi et al., 2002; Tesi et al., 2016).

5.3.3. Selective preservation and mineral protection

Particles shield OC from respiration regardless of the intrinsic recalcitrance, potentially owing to occlusion within the pore spaces that are inaccessible to microorganisms and their extracellular enzymes (Mayer, 1994; Hedges et al. 2001; Rothman and Forney, 2007). This 'mineral protection' often involves physicochemical interactions with a mineral matrix (Blattmann et al., 2019; Hemingway et al., 2019), which can be a main factor in determining the stability of marine sediments (Mayer, 1994; Keil et al., 1997; Blair and Aller, 2012). There has been evidence of mineral protection in laboratory incubation experiments (Hunter et al., 2016). Results of these experiments are characterized by non-selective OC preservation in sinking marine particles (Hedges et al., 2001), and strong correlations between OC content and mineral SSA in soils and sediments (Mayer, 1994; Vogel et al., 2014). In this study, SSA has a significant positive correlation with grain size ($r^2 = 0.53$, $P < 0.01$), showing high values from the estuary and nearshore area (Fig. 7). Therefore, higher SSA sediments are expected to have higher OC content compared with lower SSA sediments. There were significantly positive correlations with SSA among the target indices, including $nC_{14–36}$ alkanes, $nC_{25–33}$ alkanes, and $CPI_{25–33}$ (Fig. 7), suggesting that mineral protection regulates OC_{terr} at the continental margins.

Organic carbon loading and normalization of OC to particle SSA may provide a means to examine the net reaction or supply processes in particle populations independent of physical sorting (Blair and Aller, 2012). Measured OC:SSA ratios ranged from 0.06 to 1.21 mg C m^{-2}, with a mean value of 0.35 ± 0.11 mg C m^{-2}. A relatively low OC loading was predominantly observed, which reflects regions that are frequently remobilized and reoxygenated (Blair and Aller, 2012; Zhao et al., 2018). The sortable silt component of sediment that is most prone to resuspension and redistribution had relatively low OC loadings, likely

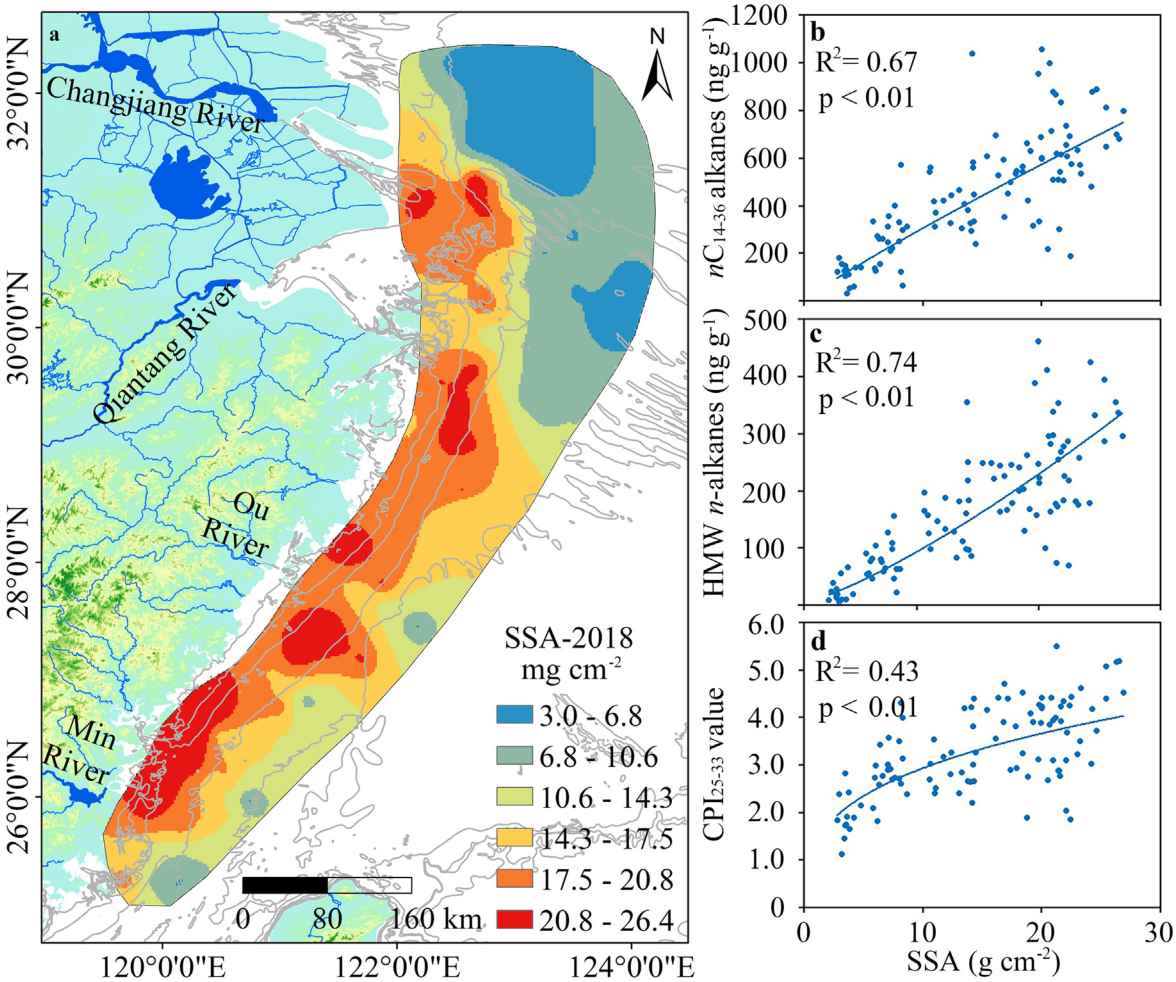

Fig. 7. a) The distribution pattern of SSA in the estuarine-inner shelf areas of the ECS; b, c, d) correlation between SSA and nC_{14-36} alkanes/ nC_{25-33} alkanes/CPI_{25-33}.

due to enhanced degradation and preferential removal of labile OC during entrainment in deposition-resuspension loops (Bao et al., 2016; 2019). The dispersal pattern of the OC:SSA ratios showed an increasing trend from nearshore to offshore, reflecting an asymptotic loading value characteristic of unstable organic-mineral associations with high reactivity and high availability for further decomposition. High OC:SSA values (>0.4 mg C m^{-2}) were mainly observed from water depths>50 m; this is consistent with an OC loading ranging from 0.4 to 1.0 mg C m^{-2} being common at depths close to in shelf sediments, due to high in situ productivity (Blair and Aller, 2012). Overall, the distribution pattern of the OC/SSA value reflects the response of OC to the hydrodynamics of the study area.

Another key factor controlling the fate of sedimentary OC may be degradation processes. This is especially the case for the OC_{terr} dispersal pattern, with marked a cross-shelf decrease of the terrestrial biomarkers such as brGDGTs, nC_{25-33} alkanes, and CPI_{25-33}, likely reflecting degradation processes during transport. If particle sorting/winnowing plays first-order control in the dispersal pattern of OC_{terr}, a similar across-shelf trend may be expected in the degradation state proxy (Tesi et al., 2014). Furthermore, it was observed that the CPI_{25-33} had a similar dispersal pattern to that of the nC_{25-33} alkanes, brGDGTs, and SSA, indicating a decreasing trend with increasing distance from the coast. The CPI measures the ratio of odd-to-even numbers for carbon chain lengths of nC_{25-33} alkanes and is based on the preference of odd carbon chain lengths for nC_{25-33} alkanes in fresh plant material (Eglinton and Hamilton, 1967). With ongoing degradation, this preference would be lost and the CPI_{25-33} would approach one (Bray and Evans, 1961). A clear decreasing trend was found for CPI_{25-33} in the cross-shelf transects 1 and 2 for 2006 and 2018, with increasing longitude (Fig. 8). The variation trend for CPI_{25-33} in the longshore transect 4 showed an increasing trend with longitude (Fig. 8). These results suggest an increase in the degradation state of OC_{terr}, with increasing distance from the coast and estuary, exhibiting degradation of labile OC during transport processes. In addition, similar dispersal patterns for CPI_{25-33} and SSA and their significant positive correlation indicate that mineral protection is another factor that controls the degradation of OC_{terr} in coastal margin sediments, as depicted in Fig. 7.

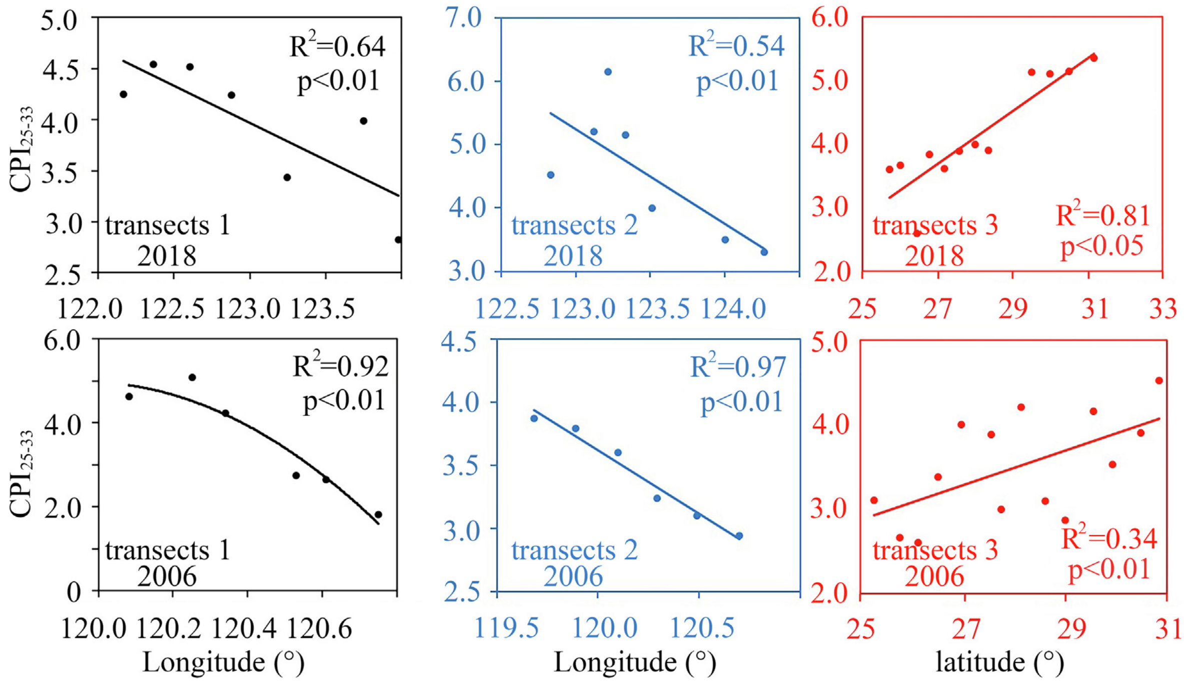

Fig. 8. Correlation $CPI_{25–33}$ value and longitude/latitude in 2006 (upper row) and 2018 (lower row); a, d) Transect 1; b, e) Transect 2; c, f) Transect 3.

5.4. The global context

These studies have demonstrated that the role of particulate OC_{terr} in the CJR-ECS S2S conveying systems has changed substantially due to anthropogenic perturbations. In this context, the role of river-dominated marginal seas as an important OC sinks is changing, and more attention should be paid to this new issue. The CJR-ECS S2S conveying system is not the only large system experiencing intensive human interference and substantial sediment load reduction. Almost all the world's river-dominated marginal seas have been or are experiencing this threat. For example, the sediment supply to the sea from the Nile River has nearly vanished because of the sediment trapping effects of the New Aswan Dam, and sediment deposition in the deltaic channel networks (Stanley, 1996), which have triggered erosion of estuarine shoals and subaqueous deltas (Blum and Roberts, 2009). Dams and river engineering activities have caused sediment load reduction from approximately 400 Mt yr^{-1} to 145 Mt yr^{-1} in the Mississippi River (Meade and Moody, 2010), resulting in delta erosion and shoreline retreat (Blum and Roberts, 2009; Maloney et al., 2018). The Yellow River, once the most sediment-laden river in the world, has experienced a sediment flux reduction from 1,221 Mt yr^{-1} in the 1950 s to 143 Mt yr^{-1} in the 2000 s, because of reforestation and reservoir construction (Wang et al., 2007; Wu et al., 2020). This has also resulted in delta erosion and sediment coarsening (Liu et al., 2022). Similar sediment load reductions have occurred in the Mekong River due to recent hydropower dam construction (Kummu et al., 2010; Schmitt et al., 2017), triggering rapid delta erosion (Anthony et al., 2015; Li et al., 2017). Other large rivers such as the Amazon River (Latrubesse et al., 2017), Ebro River (Tena and Batalla, 2013), and Ganges-Brahmaputra River system (Rahman et al., 2018) have also shown a substantial decrease in sediment flux. In addition to large rivers, hydroelectric dams have demonstrably affected the stability of small and medium river estuaries, resulting in a rapid coastal recession in what would otherwise have been accretional coastlines (Ezcurra et al., 2021). Therefore, variation in sediments in the river-marginal sea system due to human disturbances has become universal.

These global reductions in sediment loads have reduced the influx of particulate OC to ocean margins (Syvitski et al., 2005; Regnier et al., 2013; Maavara et al., 2017). This has changed the sources, compositions, dispersal, and deposition of OC in these areas. In addition, coastal erosion and seabed erosion caused by insufficient sediment supply has resulted in sediment (re)mobilization and the scouring of OC associated with fine-grained sediments. The effects of these processes may be more pronounced in the RiOMar, especially at passive margins with broad continental shelves, resulting in prolonged oxygen exposure during resuspension–deposition loops. This may, in turn, promote lateral redistribution and degradation of OC (Blair & Aller, 2012; Bao et al., 2018). Therefore, the cumulative impact of reduced riverine input coupled with seabed erosion and associated OC degradation should be re-evaluated; if this is not done, biogeochemical processes affecting OC in the RiOMar will be further complicated. Further studies should be conducted to examine the effects of intense anthropogenic perturbations on the fate of sedimentary OC in river-dominated coastal margins at the global scale.

6. CONCLUSIONS

In this study, lipid molecular biomarkers, including *n*-alkanes and GDGTs, were used as tracers for land-derived materials to investigate the influences of human-induced catchment changes on the fate of OC_{terr} along the CJR-ECS continuum. The distribution of bulk OC properties and biomarkers indicated that OC_{terr} transport in the study basin has changed due to hydraulic engineering, which also affected the provenance of the OC_{terr} discharged into the ECS. The C/N ratio, $\delta^{13}C$ value, and *n*-alkane levels indicated that in situ productivity has become an important contributor to OC_{terr} in the river SPM due to reservoir interception. Additionally, reduction in sediment loads has resulted in coarser surficial sediments in the estuarine-inner shelf areas of the ECS, which affects the delivery, dispersal, and deposition of OC_{terr}. Moreover, the TOC, *n*-alkane, and GDGT concentrations in the surficial sediments have decreased substantially. The reduction in sediment loads is one reason for this change, and hydrodynamic sorting caused by the change in the sedimentary environment is another. These conclusions are supported by positive correlations between sediment grain size and the target biomarkers. Regional circulation patterns control the dispersal and deposition of sediments and the associated OC_{terr}, resulting in the alongshore and cross-shelf transport of OC_{terr}, which undergoes degradation during its transit. Overall, anthropogenic perturbations can affect the fate of OC_{terr} by both reducing terrestrial inputs and changing the sedimentary environment. Indeed, the variation in the fate of OC_{terr} resulting from this suite of processes is likely prevalent globally. Humans have transformed the mobilization, transport and sequestration of sediment, resulting in terrestrial inputs and sedimentary environment of RiOMar having been changed on a global scale. These changes will inevitably affect the fate of sedimentary OC in the RiOMar, shaping our understanding of global OC cycling. Further global-scale studies examining the impacts of anthropogenic perturbations on the fate of sedimentary OC in RiOMar are necessary.

DECLARATION OF COMPETING INTEREST

The authors declare that they have no known competing financial interests or personal relationships that could have appeared to influence the work reported in this paper.

ACKNOWLEDGEMENTS

The study was supported by the Natural Science Foundation of China (Grant Nos. 42106056 and U2240220), the China Postdoctoral Science Foundation (Grant Nos. 2021M691504), the Fundamental Research Funds for the Central Universities (Grant Nos. 0209-14370404, 0209-14280092), Innovation Program of Shanghai Municipal Education Commission (2019-01-07-00-05-E00027), State Key Laboratory of Marine Geology, Tongji University (Grant Nos. MGK202111), and the Open Research Foundation of Key Laboratory of Marine Ecosystem Dynamics (Grant Nos. MED202009). We also thank the three anonymous reviewers and Editors for their review and constructive comments.

APPENDIX A. SUPPLEMENTARY MATERIAL

Supplementary material to this article can be found online at https://doi.org/10.1016/j.gca.2022.07.012.

REFERENCES

Bao R., Mcintyre C., Zhao M., Zhu C., Kao S. and Eglinton T. (2016) Widespread dispersal and aging of organic carbon in shallow marginal seas. *Geology* **44**(10), G37948.1.

Bao R., van der Voort T., Zhao M., Guo X., Montlucon D., McIntyre C. and Eglinton T. (2018) Influence of hydrodynamic processes on the fate of sedimentary organic matter on continental margins. *Global Biogeochem. Cycles.* **32**, 1420–1432.

Bao R., Blattmann T., McIntyre C., Zhao M. and Eglinton T. (2019) Relationships between grain size and organic carbon 14C heterogeneity in continental margin sediments. *Earth Planet. Sci. Lett.* **505**, 76–85.

Bao H., Wu Y., Zhang J., Deng B. and He Q. (2014) Composition and flux of suspended organic matter in the middle and lower reaches of the Changjiang (Yangtze River) — impact of the three gorges dam and the role of tributaries and channel erosion. *Hydrol. Process.* **28**(3), 1137–1147.

Bauer J., Cai W., Raymond P., Bianchi T., Hopkinson C. and Regnier P. (2013) The changing carbon cycle of the coastal ocean. *Nature* **504**, 61–70.

Belicka L., Macdonald R. and Harvey H. (2002) Sources and transport of organic carbon to shelf, slope, and basin surface sediments of the Arctic Ocean. *Deep-Sea Research I* **49**(8), 1463–1483.

Berner R. (1990) Atmospheric carbon dioxide levels over Phanerozoic time. *Science* **249**(4975), 1382–1386.

Berner R. (2004) *The Phanerozoic Carbon Cycle: CO_2 and O_2*. Oxford Univ. Press, New York.

Bianchi T. (2011) The role of terrestrially derived organic carbon in the coastal ocean: a changing paradigm and the priming effect. *Proc. Natl. Acad. Sci.* **108**, 19473–19481.

Bianchi T. and Allison M. (2009) Large-river delta-front estuaries as natural "recorders" of global environmental change. *Proc. Natl. Acad. Sci.* **106**, 8085–8092.

Bianchi T., Cui X., Blair N., Burdige D., Eglinton T. and Galy V. (2018) Centers of organic carbon burial and oxidation at the land-ocean interface. *Org Geochem.* **115**, 138–155.

Blaga C., Reichart G., Heiri O. and Sinninghe Damsté J. (2009) Tetraether membrane lipid distributions in water-column particulate matter and sediments: a study of 47 European lakes along a north–south transect. *J. Paleolimnol.* **41**, 523–540.

Blair N. and Aller R. (2012) The fate of terrestrial organic carbon in the marine environment. *Ann. Rev. Marine Sci.* **4**, 401–423.

Blair N., Leithold E. and Aller R. (2004) From bedrock to burial: the evolution of particulate organic carbon across coupled watershed-continental margin systems. *Mar. Chem.* **92**, 141–156.

Blattmann T., Liu Z., Zhang Y., Zhao Y., Haghipour N., Montlucon D., Plotze M. and Eglinton T. (2019) Mineralogical control on the fate of continentally derived organic matter in the ocean. *Science* **366**, 742–745.

Blum M. and Roberts H. (2009) Drowning of the Mississippi Delta due to insufficient sediment supply and global sea-level rise. *Nature Geosci.* **2**(7), 488–491.

Bray E. and Evans E. (1961) Distribution of *n*-paraffins as a clue to recognition of source beds. *Geochim. Cosmochim. Acta* **22**(1), 2–15.

Bröder L., Tesi T., Andersson A., Semiletov I. and Gustafsson Ö. (2018) Bounding cross-shelf transport time and degradation in

Siberian-Arctic land-ocean carbon transfer. *Nat. Commun.* **9**(1), 806.

Burdige D. (2005) Burial of terrestrial organic matter in marine sediments: A re-assessment. *Global Biogeochem. Cycles* **19**, GB4011.

Canuel E., Cammer S., McIntosh H. and Pondell C. (2012) Climate change impacts on the organic carbon cycle at the land-ocean interface. *Annu. Rev. Earth Planet. Sci.* **40**, 685–711.

Cao J., Duan X., Jin X., Lian E., Yin P., Li L. and Jia G. (2020) Sedimentary core brGDGTs in the East China Sea are mainly produced in situ as evidenced by their similar distributions with brGDGTs derived from intact polar lipids. *Org Geochem.* **149**, 104095.

Chang P., Isobe A., Kang K., Ryoo S., Kang H. and Kim Y. (2014) Summer behavior of the Changjiang diluted water to the East/Japan Sea: a modeling study in 2003. *Cont. Shelf Res.* **81**, 7–18.

Dac Ve N., Fan D., Van Vuong B. and Lan Dinh T. (2021) Sediment budget and morphological change in the Red River Delta under increasing human interferences. *Mar. Geol.* **431**, 106379.

Dai S. and Lu X. (2014) Sediment load change in the Yangtze River (Changjiang): A review. *Geomorphology* **215**, 60–73.

De Jonge C., Stadnitskaia A., Hopmans E., Cherkashov G., Fedotov A. and Streletskaya I., et al. (2015) Drastic changes in the distribution of branched tetraether lipids in suspended matter and sediments from the Yenisei River and Kara Sea (Siberia): implications for the use of brGDGT-based proxies in coastal marine sediments. *Geochim. Cosmochim. Acta* **165**, 200–225.

Deemer B., Harrison J., Li S., Beaulieu J., DelSontro T., Barros N., Bezerra-Neto J., Powers S., dos Santos M. and Vonk J. (2016) Greenhouse gas emissions from reservoir water surfaces: a new global synthesis. *Bioscience* **66**, 949–964.

DeMaster D., McKee B., Nittrouer C., Qian J. and Cheng G. (1985) Rates of sediment accumulation and particle reworking based on radiochemical measurements from continental shelf deposits in the East China Sea. *Cont. Shelf Res.* **4**(1–2), 143–158.

Deng B., Zhang J. and Wu Y. (2006) Recent sediment accumulation and carbon burial in the East China Sea. *Global Biogeochem. Cycles* **20**(3), GB3014.

Eglinton G. and Hamilton R. (1967) Leaf epicuticular waxes. *Science* **156**(3780), 1322–1335.

Ezcurra E., Barrios E., Ezcurra P., Ezcurra A., Vanderplank S., Vidal O., Villanueva-Almanza L. and Aburto-Oropeza O. (2021) A natural experiment reveals the impact of hydroelectric dams on the estuaries of tropical rivers. *Sci. Adv.* **5**(3), eaau9875.

Fahl K. and Stein R. (1997) Modern organic carbon deposition in the Laptev Sea and the adjacent continental slope: Surface water productivity vs. terrigenous input. *Org Geochem.* **26**, 379–390.

Gao J., Jia J., Sheng H., Yu R., Li G., Wang Y., Yang Y., Zhao Y., Li J., Bai F., Xie W., Wang A., Zou X. and Gao S. (2017) Variations in the transport, distribution and budget of ^{210}Pb in sediment over the estuarine and inner shelf areas of the East China Sea due to Changjiang catchment changes. *J. Geophys. Res. Earth Surf.* **122**(1), 235–247.

Gao J., Jia J., Kettner A., Xing F., Wang Y., Li J., Bai F., Zou X. and Gao S. (2018) Reservoir-induced changes to fluvial fluxes and their downstream impacts on sedimentary processes: the Changjiang (Yangtze) River, China. *Quat. Int.* **493**, 187–197.

Gao J., Shi Y., Sheng H., Kettner A., Yang Y., Jia J., Wang Y., Li J., Chen Y., Zou X. and Gao S. (2019) Rapid response of the Changjiang (Yangtze) river and East China Sea source-to-sink conveying system to human induced catchment perturbations. *Mar. Geol.* **414**, 1–17.

Gao S. and Wang Y. (2008) Changes in material fluxes from the Changjiang River and their implications on the adjoining continental shelf ecosystem. *Cont. Shelf Res.* **28**(12), 1490–1500.

Guo W., Jia G., Ye F., Xiao H. and Zhang Z. (2019a) Lipid biomarkers in suspended particulate matter and surface sediments in the Pearl River Estuary, a subtropical estuary in southern China. *Sci. Total Environ.* **646**, 416–426.

Guo L., Su N., Townend L., Wang Z. and Zhu C., et al. (2019b) From the headwater to the delta: A synthesis of the basin-scale sediment load regime in the Changjiang River. *Earth-Sci Rev.* **197,** 102900.

Hartnett H., Keil R., Hedges J. and Devol A. (1998) Influence of oxygen exposure time on organic carbon preservation in continental margin sediments. *Nature* **391**, 572–574.

Hedges J., Clark W., Quay P., Richey J., Devol A. and Santo S. U. (1986) Compositions and fluxes of particulate organic material in the Amazon River. *Limnol. Oceanography* **31**, 717–738.

Hedges J. and Mann D. (1979) The characterization of plant tissues by their lignin oxidation products. *Geochim. Cosmochim. Acta* **43**, 1803–1807.

Hedges J., Keil R. and Benner R. (1997) What happens to terrestrial organic matter in the ocean? *Org Geochem.* **27**(5–6), 195–212.

Hedges J., Baldock J., Gélinas Y., Lee C., Peterson M. and Wakeham S. (2001) Evidence for non-selective preservation of organic matter in sinking marine particles. *Nature* **409**(6822), 801–804.

Hemingway J., Rothman D., Grant K., Rosengard S., Eglinton T., Derry L. and Galy V. (2019) Mineral protection regulates long-term global preservation of natural organic carbon. *Nature* **570**, 228–231.

Hopmans E., Weijers J., Schefub E., Herfort L., Sinninghe Damste J. and Schouten S. (2004) A novel proxy for terrestrial organic matter in sediments based on branched and isoprenoid tetraether lipids. *Earth Planet. Sci. Lett.* **224**, 107–116.

Hu D., Pang C., Bai H. and Wang F. (2001) *Transportation and Budget of Particulate Materials in the East China Sea, Land-Sea Interactions in Changjiang and Zhujiang Estuaries and Adjacent Waters*. Ocean Press, Beijing (in Chinese).

Hu L., Shi X., Yu Z., Lin T., Wang H., Ma D., Guo Z. and Yang Z. (2012) Distribution of sedimentary organic matter in estuarine-inner shelf regions of the East China Sea: Implications for hydrodynamic forces and anthropogenic impact. *Mar. Chem.* **142**, 29–40.

Huguet C., Hopmans E., Febo-Ayala W., Thompson D., Sinninghe Damsté J. and Schouten S. (2006) An improved method to determine the absolute abundance of glycerol dibiphytanyl glycerol tetraether lipids. *Org Geochem.* **37**, 1036–1041.

Hunter W., Niederdorfer R., Gernand R., Veuger B., Prommer J., Mooshammer M., Wanek W. and Battin T. (2016) Metabolism of mineral-sorbed organic matter and microbial lifestyles in fuvial ecosystems. *Geophys. Res. Lett.* **43**, 1582–1588.

Kao S., Lin F. and Liu K. (2003) Organic carbon and nitrogen contents and their isotopic compositions in surficial sediments from the East China Sea shelf and the southern Okinawa Trough. Deep Sea Research. Part II: Topical Studies. *Oceanography* **50**(6–7), 1203–1217.

Karlsson E., Charkin A., Dudarev O., Semiletov I., Vonk J., Sánchez-García L., Andersson A. and Gustafsson Ö. (2011) Carbon isotopes and lipid biomarker investigation of sources, transport and degradation of terrestrial organic matter in the Buor-Khaya Bay, SE Laptev Sea. *Biogeosciences* **8**, 1865–1879.

Keil R., Mayer L., Quay P., Richey J. and Hedges J. (1997) Loss of organic matter from riverine particles in deltas. *Geochim. Cosmochim. Acta* **61**(7), 1507–1511.

Keil R., Dickens A., Arnarson T., Nunn B. and Devol A. (2004) What is the oxygen exposure time of laterally transported organic matter along the Washington margin? *Mar. Chem.* **92**, 157–165.

Kummu M., Lu X., Wang J. and Varis O. (2010) Basin-wide sediment trapping efficiency of emerging reservoirs along the Mekong. *Geomorphology* **119**(3), 181–197.

Lalonde K., Mucci A., Ouellet A. and Gelinas Y. (2012) Preservation of organic matter in sediments promoted by iron. *Nature* **483**, 198–200.

Latrubesse E., Arima E., Dunne T., Park E., Baker V., Horta F., Wight C., Wittmann F., Zuanon J., Baker P., Ribas C., Norgaard R., Filizola N., Ansar A., Flyvbjerg B. and Stevaux J. (2017) Damming the rivers of the Amazon basin. *Nature* **546**, 363–369.

Li X., Bianchi T., Allison M., Chapman P., Mitra S., Zhang Z., Yang G. and Yu Z. (2012) Composition, abundance and age of total organic carbon in surface sediments from the inner shelf of the East China Sea. *Mar. Chem.* **145–147**, 37–52.

Li X., Liu J. P., Saito Y. and Nguyen V. L. (2017) Recent evolution of the Mekong Delta and the impacts of dams. *Earth-Sci. Rev.* **175**, 1–17.

Li G., Wang X., Yang Z., Mao C., West A. and Ji J. (2015) Dam-triggered organic carbon sequestration makes the Changjiang (Yangtze) River basin (China) a significant carbon sink. *J. Geophys. Res. Biogeosci.* **120**, 39–53.

Liu S., Qiao L., Li G., Li J., Wang N. and Yang J. (2015) Distribution and cross-front transport of suspended particulate matter over the inner shelf of the East China Sea. *Cont. Shelf Res.* **107**, 92–102.

Liu L., Wang H., Yang Z., Fan Y., Wu X., Hu L. and Bi N. (2022) Coarsening of sediments from the Huanghe (Yellow River) delta-coast and its environmental implications. *Geomorphology* **401**, 108105.

Liu J., Xu K., Li A., Milliman J., Velozzi D., Xiao S. and Yang Z. (2007) Flux and fate of Yangtze River sediment delivered to the East China Sea. *Geomorphology* **85**(3–4), 208–224.

Liu J., Saito Y., Kong X., Wang H., Xiang L., Wen C. and Nakashima R. (2010) Sedimentary record of environmental evolution off the Yangtze River estuary, East China Sea, during the last ~13,000 years, with special reference to the influence of the Yellow River on the Yangtze River delta during the last 600 years. *Quat. Sci. Rev.* **29**(17–18), 2424–2438.

Liu J., Xiao S., Wang C., Yang Z., Liu D., Guo X., Liu L. and Lorke A. (2021) Spatial and temporal variability of dissolved methane concentrations and diffusive emissions in the Three Gorges Reservoir. *Water Res.* **207**, 117788.

Maavara T., Lauerwald R., Regnier P. and Cappellen P. (2017) Global perturbation of organic carbon cycling by river damming. *Nat. Commun.* **2017**(8), 15347.

Maloney J., Bentley S., Xu K., Obelcz J., Georgiou I. and Miner M. (2018) Mississippi river subaqueous delta is entering a stage of retrogradation. *Marine Geol.* **400**, 12–23.

Mayer L. (1994) Relationships between mineral surfaces and organic carbon concentrations in soils and sediments. *Chem. Geol.* **114**, 347–363.

McCave I. and Hall I. (2006) Size sorting in marine muds: Processes, pitfalls, and prospects for paleoflow-speed proxies. *Geochem. Geophys. Geosyst.* **7**, Q10N05.

McKee B., Aller R., Allison M., Bianchi T. and Kineke G. (2004) Transport and transformation of dissolved and particulate materials on continental margins influenced by major rivers: Benthic boundary layer and seabed processes. *Cont. Shelf Res.* **24**(7–8), 899–926.

Meade R. and Moody J. (2010) Causes for the decline of suspended-sediment discharge in the Mississippi river system, 1940–2007. *Hydrol. Process.* **24**(1), 35–49.

Milliman J. and Farnsworth K. (2011) *River discharge to the coastal ocean: A global synthesis*. Cambridge University Press, Cambridge.

Najjar R., Herrmann M., Alexander R., Boyer E., Burdige D., Butman D., Cai W., Canuel E., Chen R., Friedrichs M., Feagin M., Griffith P., Hinson A., Holmquist J., Hu X., Kemp W., Kroeger K., Mannino A., McCallister S., McGillis W., Mulholland M., Pilskaln C., Salisbury J., Signorini S., St-Laurent P., Tian H., Tzortziou M., Vlahos P., Wang Z. and Zimmerman R. (2018) Carbon budget of tidal wetlands, estuaries, and shelf waters of eastern north america. *Global Biogeochem. Cycles* **32**, 389–416.

Ohkouchi N., Eglinton T., Keigwin L. and Hayes J. (2002) Spatial and temporal offsets between proxy records in a sediment drift. *Science* **298**(5596), 1224–1227.

Peterse F., Kim J., Schouten S., Kristensen D., Koc N. and Sinninghe Damste J. (2009) Constraints on the application of the MBT/CBT palaeothermometer at high latitude environments (Svalbard, Norway). *Org. Geochem.* **40**, 692–699.

Qi Y., Wu Y., Zhang J. and He Q. (2006) The composition and distribution of particulate and dissolved *n*-alkanes in the Chang jiang Estuary in Summer. *Acta Scientiae Circum Stantiae* **26**(8), 1354–1361 (In Chinese).

Rahman M., Dustegir M., Karim R., Haque A., Nicholls R., Darby S., Nakagawa H., Hossain M., Dunn F. and Akter M. (2018) Recent sediment flux to the Ganges-Brahmaputra-Meghna delta system. *Sci. Total Environ.* **643**, 1054–1064.

Regnier P., Friedlingstein P., Ciais P., Mackenzie F., Gruber N., Janssens I., Laruelle G., Lauerwald R., Luyssaert S. and Andersson A. (2013) Anthropogenic perturbation of the carbon fluxes from land to ocean. *Nat. Geosci.* **6**, 597–607.

Rieley G., Collier R., Jones D. and Eglinton G. (1991) The biogeochemistry of Ellesmere lake, UK. 1. Source correlation of leaf wax inputs to the sedimentary lipid record. *Organic Geochem.* **17**(6), 901–912.

Rothman D. and Forney D. (2007) Physical model for the decay and preservation of marine organic carbon. *Science* **316**(5829), 1325–1328.

Schmitt R., Rubin Z. and Kondol G. (2017) Losing ground - scenarios of land loss as consequence of shifting sediment budgets in the Mekong Delta. *Geomorphology* **294**, 58–69.

Schouten S., Hopmans, Schefuß E. and Sinninghe Damsté J. (2002) Distributional variations in marine crenarchaeotal membrane lipids: a new tool for reconstructing ancient sea water temperatures? Earth Planet. *Sci. Lett.* **204**, 265–274.

Schouten S., Ossebaar J., Brummer G., Elderfield H. and Damste J. (2007) Transport of terrestrial organic matter to the deep North Atlantic Ocean by ice rafting. *Org Geochem.* **38**, 1161–1168.

Schouten S., Hopmans E., Rosell-Mele A., Pearson A., Adam P. and Bauersachs T. (2013) An interlaboratory study of TEX86 and BIT analysis of sediments, extracts, and standard mixtures. *Geochem. Geophys. Geosyst.* **14**, 5263–5285.

Shields M., Bianchi T., Gélinas Y., Allison M. and Twilley R. (2016) Enhanced terrestrial carbon preservation promoted by reactive iron in deltaic sediments. *Geophys. Res. Lett.* **43**, 1149–1157.

Sinninghe Damsté J. (2016) Spatial heterogeneity of sources of branched tetraethers in shelf systems: The geochemistry of tetraethers in the Berau River delta (Kalimantan, Indonesia). *Geochim. Cosmochim. Acta* **186**, 13–31.

Sinninghe Damsté J., Hopmans E., Pancost R., Schouten S. and Geenevasen J. (2000) Newly discovered non-isoprenoid dialkyl diglycerol tetraether lipids in sediments Journal of the Chemical Society. *Chem. Commun.*, 1683–1684.

Sinninghe Damsté J., Rijpstra W., Hopmans E., Prahl F., Wakeham S. and Schouten S. (2002a) Distribution of membrane lipids of planktonic crenarchaeota in the Arabian Sea. *Appl. Environ. Microbiol.* **68**(6), 2997–3002.

Sinninghe Damsté J., Schouten S., Hopmans E., van Duin A. and Geenevasen J. (2002b) Crenarchaeol: the characteristic core glycerol dibiphytanyl glycerol tetraether membrane lipid of cosmopolitan pelagic crenarchaeota. *J. Lipid Res.* **43**, 1641–1651.

Stanley D. (1996) Nile delta: extreme case of sediment entrapment on a delta plain and consequent coastal land loss. *Mar. Geol.* **129**(3–4), 189–195.

Syvitski J., Vörösmarty C., Kettner A. and Green P. (2005) Impact of humans on the flux of terrestrial sediment to the global coastal ocean. *Science* **308**(5720), 376–380.

Tan F. and Edmond J. (1993) Carbon isotope geochemistry of the orinoco basin. *Estuar. Coast. Shelf Sci.* **36**(6), 541–547.

Tena A. and Batalla R. (2013) The sediment budget of a large river regulated by dams (the lower river Ebro, NE Spain). *J. Soils Sediments* **13**(5), 966–980.

Tesi T., Semiletov I., Hugelius G., Dudarev O., Kuhry P. and Gustafsson Ö. (2014) Composition and fate of terrigenous organic matter along the Arctic land–ocean continuum in East Siberia: Insights from biomarkers and carbon isotopes. *Geochim. Cosmochim. Acta* **133**, 235–256.

Tesi T., Semiletov I., Dudarev O., Andersson A. and Gustafsson Ö. (2016) Matrix association effects on hydrodynamic sorting and degradation of terrestrial organic matter during cross-shelf transport in the Laptev and East Siberian shelf seas. *J. Geophys. Res.: Biogeosci.* **121**, 731–752.

Vogel C., Mueller C., Höschen C., Buegger F., Heister K., Schulz S., Schloter M. and Kögel-Knabner I. (2014) Submicron structures provide preferential spots for carbon and nitrogen sequestration in soils. *Nature Commun.* **5**, 2947.

Wang H., Yang Z., Saito Y., Liu P., Sun X. and Wang Y. (2007) Stepwise decreases of the Huanghe (Yellow River) sediment load (1950–2005): impacts of climate changes and human activities. *Global Planetary Change* **57**(3–4), 331–354.

Wang C., Zou X., Feng Z., Hao Z. and Gao J. (2018) Distribution and transport of heavy metals in estuarine-inner shelf regions of the East China Sea. *Sci. Total Environ.* **644**, 298–305.

Wang C., Hao Z., Gao J., Feng Z., Ding Y., Zhang C. and Zou X. (2020a) Reservoir construction has reduced organic carbon deposition in the East China Sea by half since 2006. *Geophys. Res. Lett.* **47**, e2020GL087357.

Wang C., Hao Z., Feng Z., Zhang C., Li Y., Yu W. and Zou X. (2020b) Shifts in the distribution and fate of sedimentary polycyclic aromatic hydrocarbons within the estuarine-inner shelf areas of the East China Sea: Response to human-induced catchment change. *J. Geophys. Res. Oceans* **125**, e2019JC015773.

Waterson E. and Canuel E. (2008) Sources of sedimentary organic matter in the Mississippi River and adjacent Gulf of Mexico as revealed by lipid biomarker and $\delta^{13}C_{TOC}$ analyses. *Org Geochem.* **39**, 422–439.

Wei B., Mollenhauer G., Hefter J., Grotheer H. and Jia G. (2020) Dispersal and aging of terrigenous organic matter in the Pearl River Estuary and the northern South China Sea Shelf. *Geochim. Cosmochim. Acta* **282**, 324–339.

Wu X., Wang H., Bi N., Saito Y., Xu J., Zhang Y., Lu T., Cong S. and Yang Z. (2020) Climate and human battle for dominance over the Yellow River's sediment discharge: From the Mid-Holocene to the Anthropocene. *Mar. Geol.* **425**, 106188.

Wu Y., Zhang J., Liu S., Zhang Z., Yao Q., Hong G. and Cooper L. (2007) Sources and distribution of carbon within the Yangtze River system. *Estuar. Coast. Shelf Sci.* **71**, 13–25.

Weijers J., Schouten S., Spaargaren O. and Sinninghe Damsté J. (2006) Occurrence and distribution of tetraether membrane lipids in soils: implications for the use of the TEX86 proxy and the BIT index.. *Org. Geochem.* **37**, 1680–1693.

Wu Y., Eglinton T. I., Zhang J. and Montlucon D. (2018) Spatiotemporal variation of the quality, origin, and age of particulate organic matter transported by the Yangtze River (Changjiang). *J. Geophys. Res.: Biogeosci.* **123**, 2908–2921.

Xing L., Zhang H., Yuan Z., Sun Y. and Zhao M. (2011) Terrestrial and marine biomarker estimates of organic matter sources and distributions in surface sediments from the East China Sea shelf. *Cont. Shelf Res.* **31**(10), 1106–1115.

Yamamoto M., Okino T., Sugisaki S. and Sakamoto T. (2008) Late Pleistocene changes in terrestrial biomarkers in sediments fromthe central Arctic Ocean. *Org Geochem.* **39**(6), 754–763.

Yang S., Milliman J., Li P. and Xu K. (2011) 50,000 dams later: erosion of the Yangtze River and its delta. *Global Planet. Change* **75**, 14–20.

Yang S., Milliman J., Xu K., Deng B., Zhang X. and Luo X. (2014) Downstream sedimentary and geomorphic impacts of the Three Gorges Dam on the Yangtze River. *Earth-Sci. Rev.* **138**, 469–486.

Yang S., Xu K., Milliman J., Yang H. and Wu C. (2015) Decline of Yangtze River water and sediment discharge: impact from natural and anthropogenic changes. *Sci. Rep.* **5**, 12581.

Yang H., Yang S., Xu K., Milliman J., Wang H., Yang Z., Chen Z. and Zhang C. (2018a) Human impacts on sediment in the Yangtze River: a review and new perspectives. *Global Planetary Change* **162**, 8–17.

Yang H., Yang S., Meng Y., Xu K., Luo X. and Wu C., et al. (2018b) Recent coarsening of sediments on the southern yangtze subaqueous delta front: a response to river damming. *Cont. Shelf Res.* **155**, 45–51.

Yao P., Yu Z., Bianchi T., Guo Z. and Dong L. (2015) A multiproxy analysis of sedimentary organic carbon in the changjiang estuary and adjacent shelf. *J. Geophys. Res. Biogeosci.* **120**(7), 1407–1429.

Yuan D. and Hsueh Y. (2010) Dynamics of the cross-shelf circulation in the Yellow and East China Seas in winter. *Deep Sea Res. Part II* **57**(19–20), 1745–1761.

Yuan D., Qiao F. and Su J. (2005) Cross-shelf penetrating fronts off the southeast coast of China observed by MODIS. *Geophys. Res. Lett.* **32**, 2005GL023815.

Yunker M., Belicka L., Harvey H. and Macdonald R. (2005) Tracing the inputs and fate of marine and terrigenous organic matter in Arctic Ocean sediments: a multivariate analysis of lipid biomarkers. *Deep-Sea Res. II* **52**(24–26), 3478–3508.

Zell C., Kim J., Hollander D., Lorenzoni L., Baker P., Silva C., Nittrouer C. and Sinninghe Damste J. (2014) Sources and distribution of branched and isoprenoid tetraether lipids on the Amazon shelf and fan: Implications for the use of GDGT-based paleothermometers in marine sediments. *Geochim. Cosmochim. Acta* **139**, 293–312.

Zhao B., Yao P., Bianchi T., Arellano A., Wang X., Yang J., Su R., Wang J., Xu Y., Huang X., Chen L., Ye J. and Yu Z. (2018) The remineralization of sedimentary organic carbon in different sedimentary regimes of the Yellow and East China Seas. *Chem. Geol.* **495**, 104–117.

Zhao Y., Zou X., Gao J., Xu X., Wang C., Tang D., Wang T. and Wu X. (2015) Quantifying the anthropogenic and climatic contributions to changes in water discharge and sediment load into the sea: a case study of the Yangtze River, China. *Sci. Total Environ.* **536**, 803–812.

Zhu C., Weijers J., Wagner T., Pan J., Chen J. and Pancost R. (2011) Sources and distributions of tetraether lipids in surface sediments across a large river-dominated continental margin. *Org Geochem.* **42**, 376–386.

Zhu C., Wagner T., Talbot H., Weigers J., Pan J. and Pancost R. (2013) Mechanistic controls on diverse fates of terrestrial organic components in the East China Sea. *Geochim. Cosmochim. Acta* **117**, 129–143.

Associate editor: Elizabeth Ann Canuel